

1 **Reframing gullies as recharge zones in dryland landscapes of the Loess Plateau, China**

2

3 Zhenxia Ji^{a,b,c,d}, Alan D. Ziegler^e, Li Wang^{a,b,c,d}

4 ^a State Key Laboratory of Soil and Water Conservation and Desertification Control, College of Natural
5 Resources and Environment, Northwest A&F University, Yangling 712100, China

6 ^b College of Soil and Water Conservation Science and Engineering, Northwest A&F University, Yangling
7 712100, China

8 ^c State Key Laboratory of Soil and Water Conservation and Desertification Control, Chinese Academy of
9 Sciences and the Ministry of Water Resources, Yangling 712100, China

10 ^d Institute of Soil and Water Conservation, Chinese Academy of Sciences and the Ministry of Water
11 Resources, Yangling 712100, China

12 ^e Andaman Coastal Station for Research and Development, Kasetsart University, Ranong, Thailand

13

14 Correspondence to: Li Wang (wangli5208@nwsuaf.edu.cn)

15 State Key Laboratory of Soil and Water Conservation and Desertification Control, Institute of Soil and
16 Water Conservation, Northwest A&F University.

17 Address: Xinong Road, #26, Yangling, Shaanxi Province 712100, China

18

19 **Abstract**

20 Large gullies in dryland landscapes are often ~~viewed as~~ indicators of land degradation by surface
21 runoff. However, under conditions where gully systems are hydrologically arrested by restoration
22 interventions that increase water residence time—most notably check dams and ponds—they may also
23 function as hydrologically active zones of groundwater recharge and subsurface connectivity.~~However,~~
24 ~~yet in some settings they may serve critical ecohydrological functions—supporting groundwater recharge~~
25 ~~and subsurface connectivity.~~ In China’s Loess Plateau, we assess these functions in the Nianzhuang
26 Catchment using a multi-indicator, process-based approach that integrates stable isotopes ($\delta^2\text{H}$, $\delta^{18}\text{O}$),
27 chloride concentrations, and groundwater level fluctuations. Our results show that precipitation is the
28 dominant source of recharge for shallow pore water within engineered gully zones, while deeper fissure
29 water is replenished more slowly through percolation. Hydrological arrest through ecological
30 engineering interventions acts~~Restoration interventions, particularly check dams and ponds —, act~~ as
31 focal points for groundwater infiltration, enhancing recharge in otherwise limited dryland systems.
32 Estimated annual recharge in the monitored gully-zone pore aquifer —(238–241 mm) ~~accounts for over~~
33 equivalent to about 43% of the mean annual precipitation at the site, far exceeding a site-specific recharge
34 magnitude that far exceeds ~~typical reported catchment-wide recharge~~ rates observed in nearby tableland
35 and hilly areas. Our results indicate that engineered gully systems can act as focused recharge zones
36 rather than solely degraded landforms. By linking runoff convergence and ponding to measurable
37 recharge responses, the study provides a process-based framework for assessing groundwater dynamics
38 in managed semi-arid landscapes.

39

40 **Keywords:** surface water, spring water, pore water, fissure water, hydrological connectivity, groundwater
41 recharge

42

43 **1. Introduction**

44 Groundwater recharge is a critical yet poorly understood component of hydrological cycles in
45 dryland catchments (Li et al., 2024a). It is shaped by the precipitation regime, surface landcover
46 heterogeneity, ~~the~~ integrity of the subsurface regolith, ~~the~~ characteristics of the underlying bedrock, and
47 human interventions (Vries and Simmers, 2002; Owuor et al., 2016; Salek et al., 2018; Xu and Beekman,

2019; Zhang et al., 2020; Li et al., 2024b; Medici et al., 2024). While favorable subsurface flow pathways can locally enhance recharge, dryland regions are highly sensitive to even slight changes in precipitation, soil moisture, or runoff generation. This heightened sensitivity reflects their position along climatic ecotones and the influence of complex land–atmosphere–biosphere feedbacks (Kuang et al., 2019; Al-Oqaili et al., 2020; He et al., 2020; Jin et al., 2019; Jia et al., 2024). Small changes in these processes can cascade across catchments at various scales, amplifying existing vulnerabilities to ecological and social systems (Nicholson, 2011; Huang et al., 2017; Berg et al., 2016). ~~Although favorable subsurface flow pathways can locally enhance recharge, dryland regions—situated along climatic ecotones and shaped by complex land–atmosphere–biosphere feedbacks—are highly sensitive to even modest shifts in water availability. Small changes in soil moisture or runoff routing can cascade across catchments at various scales, amplifying existing vulnerabilities to ecological and social systems (Nicholson, 2011; Huang et al., 2017; Berg et al., 2016).~~ In these fragile landscapes, understanding groundwater replenishment processes—affected collectively by vegetation, geomorphology, and engineering—is crucial for key to sustaining ecosystems, securing water, and guiding restoration and management. ~~In these “fragile” and diverse landscapes, understanding the processes that govern when, where, and how groundwater is replenished—including the countervailing influences of vegetation dynamics, geomorphology, and engineered features—is essential for sustaining ecosystems, securing water resources, and informing land restoration and catchment management (Gleeson et al., 2016; Jasechko and Perrone, 2021; Scanlon et al., 2006).~~

Despite a growing body of research on groundwater recharge in (semi-) arid regions, significant knowledge gaps remain in landscapes with pronounced spatial heterogeneity—, such as slopes, hilltops, and ~~gullies~~ gully systems—, where infiltration pathways and recharge processes can diverge sharply over short distances (Tooth, 2012; Manna et al., 2018; Letz et al., 2021). Gully systems, often seen as signs of land degradation, may paradoxically beneficially act as recharge zones, capturing and infiltrating surface runoff during episodic rainfall. ~~Among these landforms, gully systems—often regarded as hallmarks of land degradation—may paradoxically serve as focal points for recharge, capturing and infiltrating surface runoff during episodic rainfall events (Tan et al., 2017; Li et al., 2024a; Xue et al., 2025).~~ However, this same topographic focusing enables the rapid downslope transport of contaminants, including agricultural nutrients, sediments, and associated pollutants. ~~Notably, gully systems may facilitate the rapid downslope transport of contaminants such as agricultural contaminants and sediments~~

78 (Lian et al., 2025; Qu et al., 2025). However, the role of gullies in promoting vertical infiltration into
79 groundwater is highly dependent on local subsurface connectivity and permeability conditions. Moreover,
80 their broader hydrological functions remain poorly quantified—, especially under the influence of
81 widespread human interventions such as check dams and artificial ponds. While these structures are
82 typically designed to arrest land [surface](#) degradation, they can substantially alter surface–subsurface
83 connectivity and reshape recharge dynamics [in uncertain ways](#) (Lamontagne et al., 2021; [Huang et al.,](#)
84 [2019](#); Wang et al., 2023).

85 ~~This study addresses these issues by focuses focusing on groundwater recharge in the gully systems~~
86 ~~in temperate loess soils.~~ Worldwide, loess covers approximately 6% of the land surface area, forming
87 discontinuous east–west belts in the mid-latitude forest-steppe, steppe, and desert-steppe zones of both
88 hemispheres (Liu, 1985; Pécsi, 1990; Li et al., 2020). Among these, the Chinese Loess Plateau, [the focus](#)
89 [of our study](#) accounts for approximately 7.4% of the global loess area (635,280 km²; Li et al., 2020).
90 ~~It serves as a globally important natural laboratory for studying soil erosion and groundwater recharge~~
91 ~~processes, due to its exceptionally thick loess deposits (Li et al., 2021), highly erodible soils, intense~~
92 ~~summer rainstorms, and long history of agricultural activity, which collectively make it one of the most~~
93 ~~severely eroded regions worldwide (Shi and Shao, 2000; Fu et al., 2011). Its distinctive stratigraphic~~
94 ~~structure, characterized by thick, low-permeability loess layers, fundamentally governs groundwater~~
95 ~~behavior (Qiao et al., 2017). Meanwhile, extensive human interventions aimed at erosion control,~~
96 ~~including large-scale afforestation and gully engineering projects, have profoundly altered regional~~
97 ~~hydrological processes and the spatial redistribution of water (Wang et al., 2020; Zhao et al., 2024).~~

98 The setting for our investigation [is a](#) semi-arid landscape [that](#) has been shaped by severe soil erosion,
99 extensively modified by engineered landforms; and it is now characterized by chronic water scarcity (Fu
100 et al., 1999; Liu et al., 2017; Liu and Li, 2017; Li et al., 2021; [Huang et al., 2024](#)). [Water scarcity](#)
101 ~~manifests~~[manifests as](#) ~~as~~ [declining groundwater levels, reduced streamflow, dried-up wells and springs,](#)
102 [and limited irrigation capacity \(Yu et al., 2025\).](#) In such vulnerable environments, understanding the
103 sources and sustainability of groundwater recharge is critical for long-term water resource management
104 (Ajjur and Baalousha, 2021; Meles et al., 2024). Groundwater, [for example](#), is a lifeline for rural
105 communities in the hilly–gully region, yet scientific attention has largely bypassed the gullies themselves.
106 ~~Most previous studies have focused on recharge processes in tablelands and loess-covered hills,~~
107 ~~highlighting slow “piston flow” as the dominant mechanism (Huang and Pang, 2011; Huang et al., 2013;~~

108 Li et al., 2017; Lu, 2020; Wang et al., 2024). However, the deep-profile recharge mechanisms observed
109 in these areas may not apply to the gully-dominated landscapes of the Loess Plateau (Wang et al., 2024;
110 Qiao et al., 2017; Zhu et al., 2018). Moreover, the hydrological functions of widely distributed gully
111 systems, especially under the influence of engineering structures such as check dams, remain
112 insufficiently quantified, and their underlying processes have long remained in the research shadow (Liu
113 et al., 2011). Most prior research has centered on recharge processes in tablelands and loess-covered hills
114 (Huang et al., 2011; Li et al., 2017; Lu, 2020; Wang et al., 2024), leaving the hydrological role of gully
115 systems—despite their striking prominence in the landscape—largely in the shadows uncharted (Liu et
116 al., 2011).

117 Therefore, ~~in this study, we~~ his study selects the Nianzhuang Catchment, a typical gully area on
118 the Loess Plateau impacted by check dams, to establish a multi-method framework for assessing
119 groundwater recharge by integrating ~~integrate~~ stable isotope analysis ($\delta^2\text{H}$ and $\delta^{18}\text{O}$), chloride
120 concentrations, water table fluctuations, and hydro-statistical modeling ~~to establish a multi method~~
121 framework for assessing groundwater recharge in gully systems of the Loess Plateau. Specifically, our
122 goals are to ~~we aim to~~: (1) characterize the isotopic and hydrochemical signatures of precipitation, surface
123 water (ponds), shallow pore water, and deeper fissure water; (2) identify and trace hydraulic connections
124 and flow paths of different water bodies ~~trace hydraulic connections, flow paths, and recharge~~
125 mechanisms ~~distinguishing topographic focused recharge in gullies from dispersed piston flow~~
126 recharge on hillslopes; and (3) quantitatively estimate pore-water recharge rates ~~quantitatively estimate~~
127 pore water recharge rates while evaluating uncertainties and the amplifying role of restoration
128 interventions (check dams and ponds). ~~By reconciling potential contradictions among methods and~~
129 acknowledging risks such as enhanced pollutant transport, this complementary approach reframes gullies
130 as critical recharge zones in engineered dryland landscapes, providing actionable insights for sustainable
131 groundwater management and ecological restoration in the Loess Plateau and similar semi-arid regions
132 worldwide.

133 In this study, we ~~integrate stable isotope analysis ($\delta^2\text{H}$ and $\delta^{18}\text{O}$), chloride concentration~~
134 measurements, water table fluctuation estimations, and hydro-statistical modeling to do the following: (i)
135 quantify pore water recharge rates; and (ii) trace flow paths among surface water, pore water, and fissure
136 water. This integrated approach aims to advance understanding of groundwater dynamics in complex
137 dryland terrains, ~~reframes gullies~~ engineered gully systems as critical recharge zones in engineered

138 dryland landscapes, providing actionable insights for sustainable groundwater management and
139 ecological restoration in the Loess Plateau and similar semi-arid regions worldwide.~~generating process-~~
140 ~~based insights critical for sustainable water and land management in gully dominated systems—not only~~
141 ~~across the Loess Plateau, but in drylands globally.~~

142

143 **2. Hydro geomorphological processes of the Loess Plateau**

144 The Loess Plateau in China stands out as one of the most ecologically and hydrologically distinctive
145 landscapes in the world (Fu et al., 2017). Spanning over 640,000 km², it harbors the planet's largest and
146 deepest loess deposits and has long served as a cradle of Chinese civilization (Li et al., 2021). The Loess
147 Plateau is also one of the most severely eroded regions in the world, shaped by the interplay of highly
148 erodible soils, intense summer storms, and a long history of farming on sloping lands (Shi and Shao,
149 2020). For centuries, steep hillslopes were cultivated without adequate soil conservation, removing
150 vegetation and exposing loess soils to heavy runoff during short, high intensity monsoonal rains. These
151 conditions led to widespread gully formation—hallmarks of degradation tightly linked to land use and
152 rainfall extremes (Wang et al., 2006; Fu et al., 2011; Jin et al., 2020). The altered hydrological cycle on
153 the plateau has led to sharp declines in both streamflow and groundwater levels, resulting in acute water
154 scarcity across this arid to semi arid region (200–750 mm annual rainfall) (Liang et al., 2015; Wang et
155 al., 2023; Chen et al., 2023). Understanding hydrological processes in this disturbed setting is essential
156 for ~~guiding soil conservation, optimizing groundwater recharge, and ensuring the long term~~
157 ~~sustainability of water resources for both people and ecosystems.~~

158 The plateau's complex stratigraphy, with loess layers up to 350 meters deep and an average of 90
159 meters, governs groundwater storage, recharge processes, and subsurface flow due to its low
160 permeability~~The plateau's complex stratigraphy—characterized by loess layers that can reach depths of~~
161 ~~up to 350 meters and average around 90 meters, with generally low permeability—governs groundwater~~
162 ~~storage, recharge processes, and subsurface flow behavior (Qiao et al., 2017; Zhu et al., 2018). The region~~
163 ~~is further divided into a range of distinctive landforms, or subregions, also shaped by variable erosion~~
164 ~~processes (Yang et al., 2009): Loess Yuan (flat, high elevation tablelands); Loess Liang (elongated~~
165 ~~ridges); Loess Mao (rounded or oval shaped hills); general types of hills; and large scale gullies (Fig.~~
166 ~~A1). While the Loess Yuan remains relatively unincised by rivers/streams and maintains a smooth surface~~

167 morphology, the Liang and Mao formations exhibit profound dissection—shaped predominantly by
168 fluvial erosion and hillslope processes, respectively.—

169 Hills in the region exhibit undulating terrain shaped by prolonged weathering and diffuse surface
170 runoff. In contrast, gully systems reflect both long term geomorphic evolution and more recent
171 intensification driven by human activity—making them products of millennial scale natural processes
172 and modern land use pressures (Li et al., 2021; Jia et al., 2024). Prominent gully systems, which can
173 stretch for several kilometers, serve as primary conduits for concentrated runoff, facilitating the
174 downslope transfer of water, sediment, and eroded material. In doing so, they reflect and reinforce
175 ongoing landscape evolution and contribute to downstream sedimentation challenges (Zhu et al., 2018).

176 To combat degradation in the hilly and gully regions, afforestation has been carried out on hillslopes,
177 and hydraulic structures like check dams and ponds have been built in gulliesTo combat degradation in
178 the hilly gully region, extensive afforestation efforts have been implemented on hillslopes, while
179 hydraulic structures—including check dams and ponds—have been constructed in gullies (Feng et al.,
180 2016; Xue et al., 2025). These interventions have significantly altered runoff dynamics and water budgets
181 (Huang et al., 2013; Yuan et al., 2022). While afforestation has reduced soil moisture in hilly areas via
182 enhanced evapotranspiration (−8.7%), hydraulic engineering has increased soil moisture in gullies by 21%
183 (Wang et al., 2019, 2020; Zhao et al., 2019, 2024). Notably, the additional water retained within gully
184 systems offsets an estimated 44% of the water loss from afforested hillslopes, partially reshaping the
185 local water cycle (He et al., 2020; Zhao et al., 2024). Under such intensive human modification, the
186 Plateau's inherently complex landforms and stratigraphy have come to exert even greater control over
187 groundwater recharge dynamics (Li et al., 2024).

188 Research on groundwater recharge in the Loess Plateau's gully regions is incomplete, with most
189 studies concentrating on deep profiles in tableland and hilly areas (Huang et al., 2011; Li et al., 2017; Lu,
190 20212020; Wang et al., 2024). Early scholars proposed that fissures and caves in loess enabled
191 preferential flow, allowing precipitation to reach groundwater (Yan and Wang, 1983). However, Xu et al.
192 (1993) argued that the vertical fractures in the loess layer do not facilitate continuous water movement;
193 instead, the vertical joints and large pores may act as barriers, which is caused by air blocking effects. Li
194 (2001) argued that the formation of dried soil layers further disrupts groundwater recharge pathways,
195 causing precipitation to cycle within the soil-plant-atmosphere system rather than contributing
196 meaningfully to groundwater recharge. In recent years, researchers have applied isotope tracing,

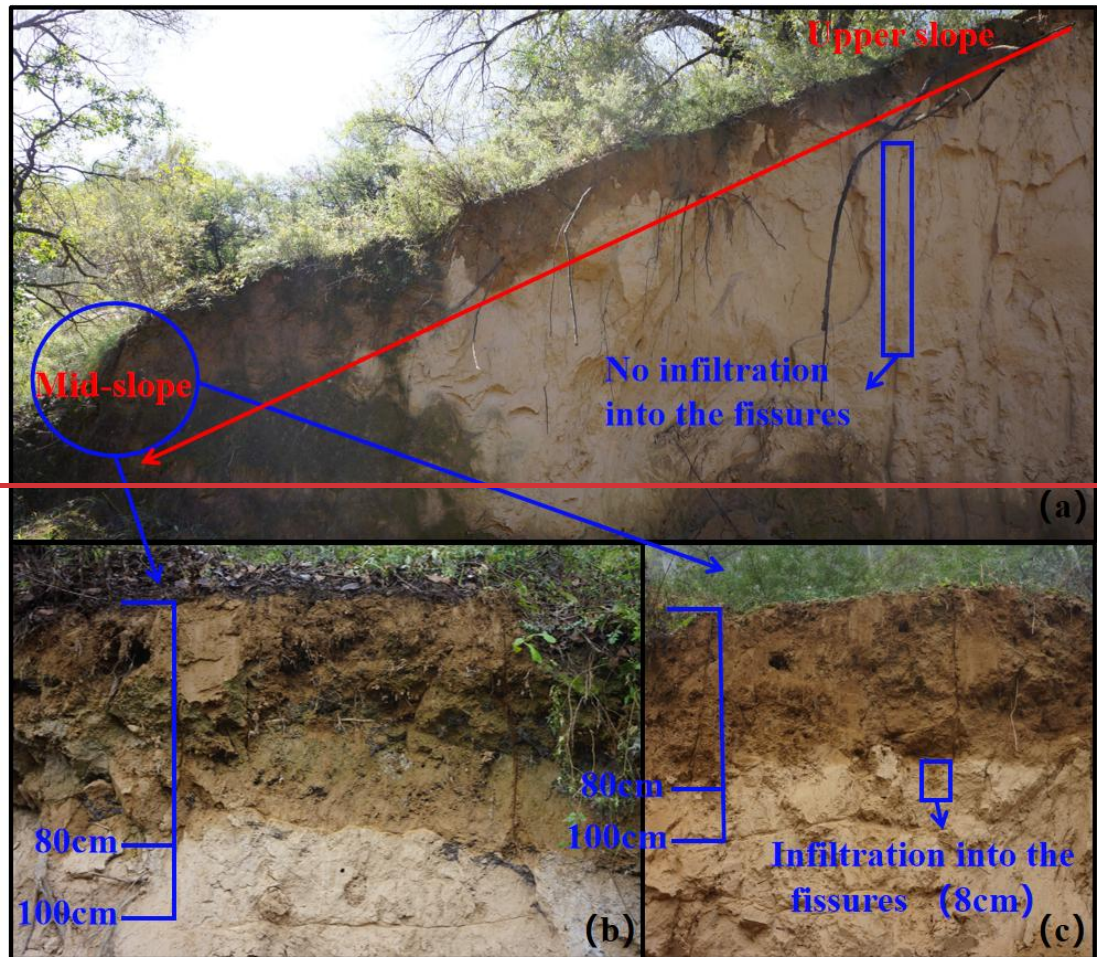
197 hydrochemical analysis, and model simulations to study recharge mechanisms in deep loess regions (Lu,
198 2020; Xiang, 2020; Shi et al., 2021; Wang et al., 2023). These studies suggest that recharge occurs
199 primarily through slow piston flow, with precipitation infiltrating thick soil profiles, slowly recharging
200 groundwater in a process that can take decades to hundreds of years (Huang et al., 2013; Tan et al., 2017;
201 Li et al., 2024). Piston flow describes the displacement of pre-existing water by newly infiltrating water,
202 moving frontally through the pore spaces refers to a type of water movement through the unsaturated
203 (vadose) zone or an aquifer where newly infiltrating water pushes the existing water downward, much
204 like a piston in a cylinder (Gee and Hillel, 1988).

205 However, deep-profile recharge mechanisms observed in tableland and hilly areas may not apply to
206 gully landscapes on the plateau. Regional scale analyses of 40 years of soil moisture data show that
207 precipitation infiltration in thick loess deposits is typically restricted to shallow depths, even though loess
208 thickness in tableland and hilly areas ranges from 56.5 to 204.5 m (Wang et al., 2024; Qiao et al., 2017).
209 In contrast, loess in gully regions is generally much thinner—often less than 50 m (Zhu et al., 2018).
210 Infiltration on loess slopes appears similarly limited (Fig. 1).

211 During field observations in the 2023 rainy season in the Nianzhuang Catchment, located in the
212 hilly gully region of the Loess Plateau plateau, we found little evidence of preferential flow through
213 cracks or macropores. Instead, infiltration appeared slow and driven predominantly by percolation
214 through the matrix (Wang et al., 2024). That year, total rainfall from May to October amounted to 420
215 mm, with 115 mm falling in September alone. Consistent with earlier studies (Xu et al., 1993; Li, 2001),
216 only a few surface cracks showed signs of infiltration, and even then, the water was absorbed by
217 surrounding soils and failed to infiltrate deeper (Fig. 1c). Moreover, soil profiles remained unsaturated
218 from the surface to deeper layers, indicating that precipitation infiltration is generally insufficient to
219 recharge groundwater (Qiao et al., 2017). After a 41-mm rainfall event occurring over four days,
220 infiltration depths reached only 20–30 cm at the top of the slope, compared with 80 cm at mid-slope
221 positions (Fig. 1b, e).

222 These patterns indicate that infiltration is limited at higher slope elevations, with much of the water
223 moving laterally downslope as overland flow and accumulating in gully areas, where conditions are more
224 conducive to groundwater recharge. Previous studies have shown that gullies and other topographic
225 depressions function as key recharge zones, enabling concentrated surface flows to infiltrate more deeply
226 and contribute to subsurface water stores (Gates et al., 2011; Liu et al., 2011; Zhao et al., 2021). Building

227 on this foundation, advancing our understanding of gully driven recharge requires targeted investigation
 228 of interactions among precipitation, surface water, and groundwater — particularly the flow paths and
 229 magnitudes of near surface infiltration. These insights are critical for guiding water resource
 230 management and ecological restoration across the Loess Plateau region.



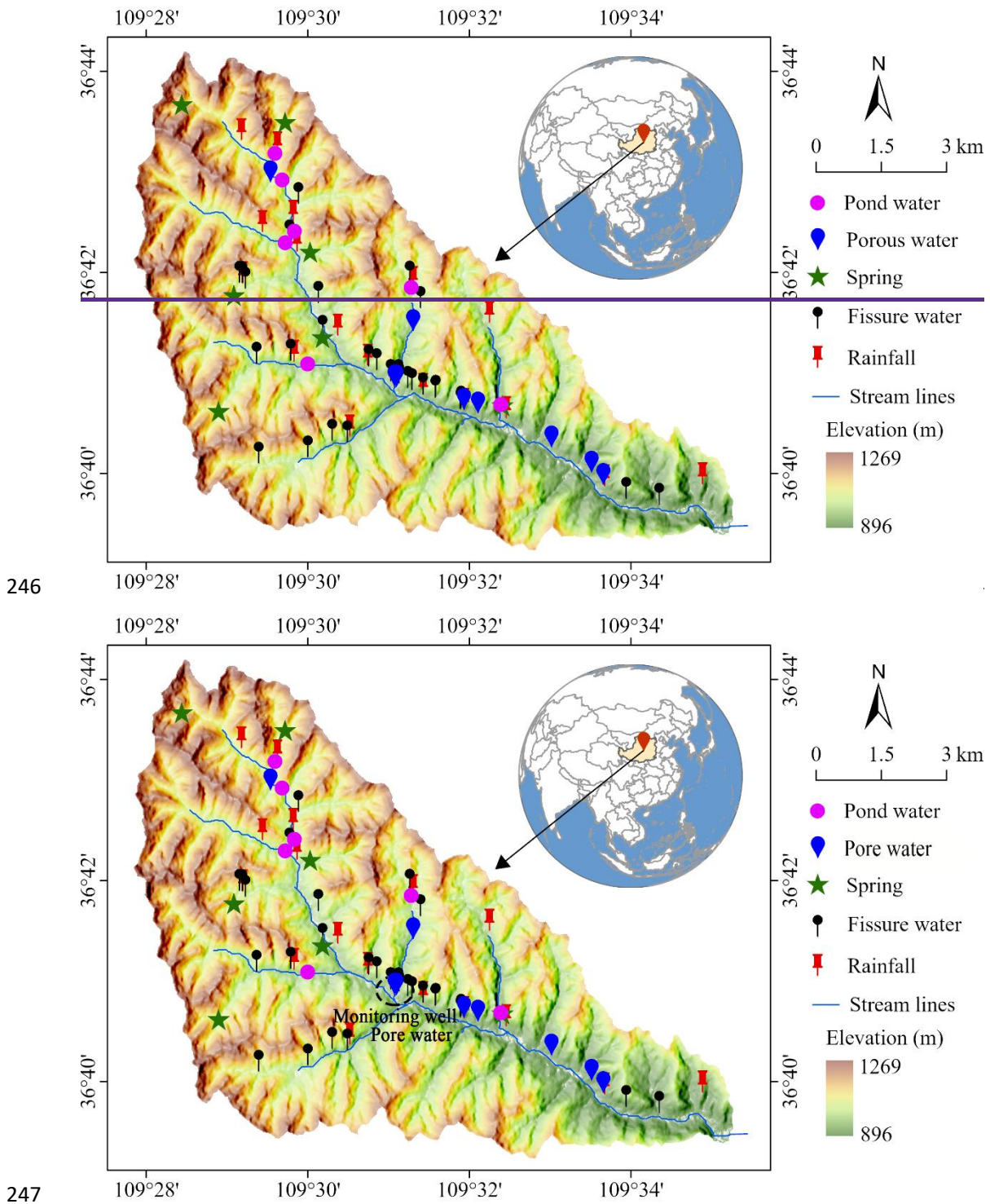
231
 232 Fig. 1. The topographic profile of the Nianzhuang catchment in the hilly region of the Loess Plateau. Full
 233 profile from the top to mid-slope (a); two repeated mid-slope profiles (b, c). The photo was taken after a
 234 41 mm rainfall event over four days. Subsequent measurements showed that infiltration depths reached
 235 only 20–30 cm at the top of the slope, compared to approximately 80 cm at the mid-slope positions.

236

237 **3.2. Sampling site**

238 The Nianzhuang Catchment is located northwest of Yan'an City in Shaanxi Province, China
 239 (approximately 36°42'N, 109°31'E). As a tributary of the Yanhe River — which ultimately flows into the
 240 Yellow River — the catchment spans 53.94 km² and includes the well-studied Yangjuangou sub-

241 catchment (3.11 km²; ~36°35'N, ~109°32'E), previously investigated in numerous hydrological and
 242 ecological studies (Fu et al., 1999; [Fu et al., 2011](#); [Fu et al., 2017](#); Liu and Li, 2017). Elevation ranges
 243 from 896 to 1,269 m, with terrain gradually sloping from northwest to southeast (Fig. 21). The region
 244 experiences a semi-arid continental monsoon climate, with a mean annual precipitation of approximately
 245 550 ± 100 mm, concentrated between July and September (Liu et al., 2017).



248 Fig. 21. The geographical location and sampling sites for rainfall, pond water, pore water, spring water,

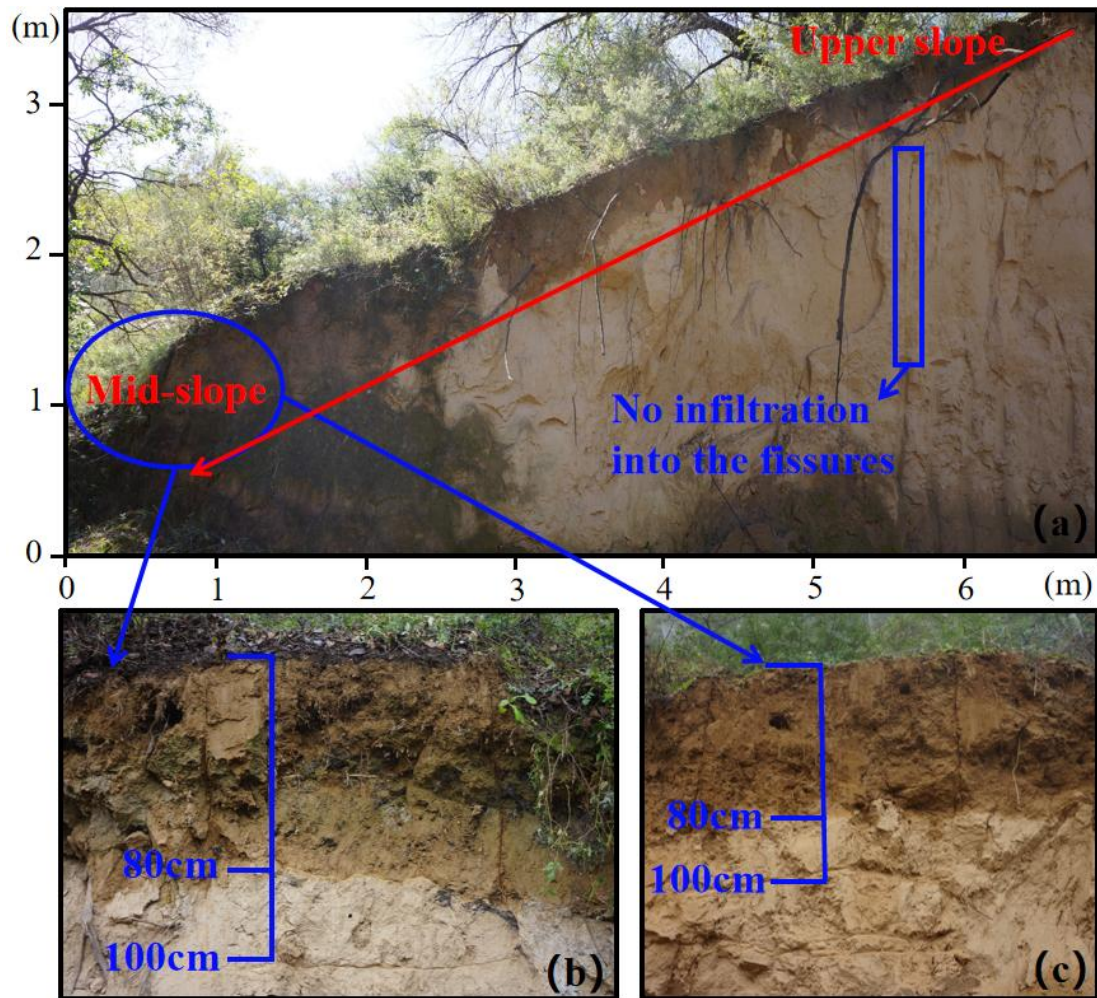
249 and fissure water in the Nianzhuang ~~catchment~~Catchment. The Nianzhuang ~~catchment~~Catchment is
250 located in the hilly and gully region of the central Loess Plateau, with elevations ranging from ~~869-896~~
251 to 1269 m. The average depth of pore water wells is 8.0 ± 1.5 m (range: 4–10 m), while that of fissure
252 water wells is 57.6 ± 29.2 m (range: 25–170 m). These sampling sites represent locations where both
253 rainy and dry season samples were collected, and are all situated within the gully areas of the catchment.

254

255

256 The catchment features highly dissected loess terrain, with characteristic soils and landforms such
257 as Loess Liang (ridges), Loess Mao (mounds), and steep loess slopes (Cai et al., 2019). Gullies—, often
258 “V”- or “U”-shaped—, dominate the lower-lying regions and serve as important recharge zones. These
259 landforms, together with ancient landslides, minor collapses, and sinkholes, highlight the geomorphic
260 instability of the Loess Plateau landscape (Li et al., 2021).

261 From May to October 2023, total rainfall reached 420 mm, with 115 mm in September alone. Despite
262 this substantial precipitation, field observations revealed shallow infiltration depths on loess slopes even
263 after heavy rainfall events of up to 41 mm. Infiltration was limited to 20–30 cm at hilltops and about 80
264 cm at mid-slope, with no distinct preferential flow and largely unsaturated soil profiles (Fig. 2). These
265 observations suggest that groundwater recharge occurs mainly through surface or near-surface runoff
266 converging into gullies/engineered gully systems, underscoring their critical role as focused zones of
267 groundwater recharge and key natural sites for studying these processes.



268

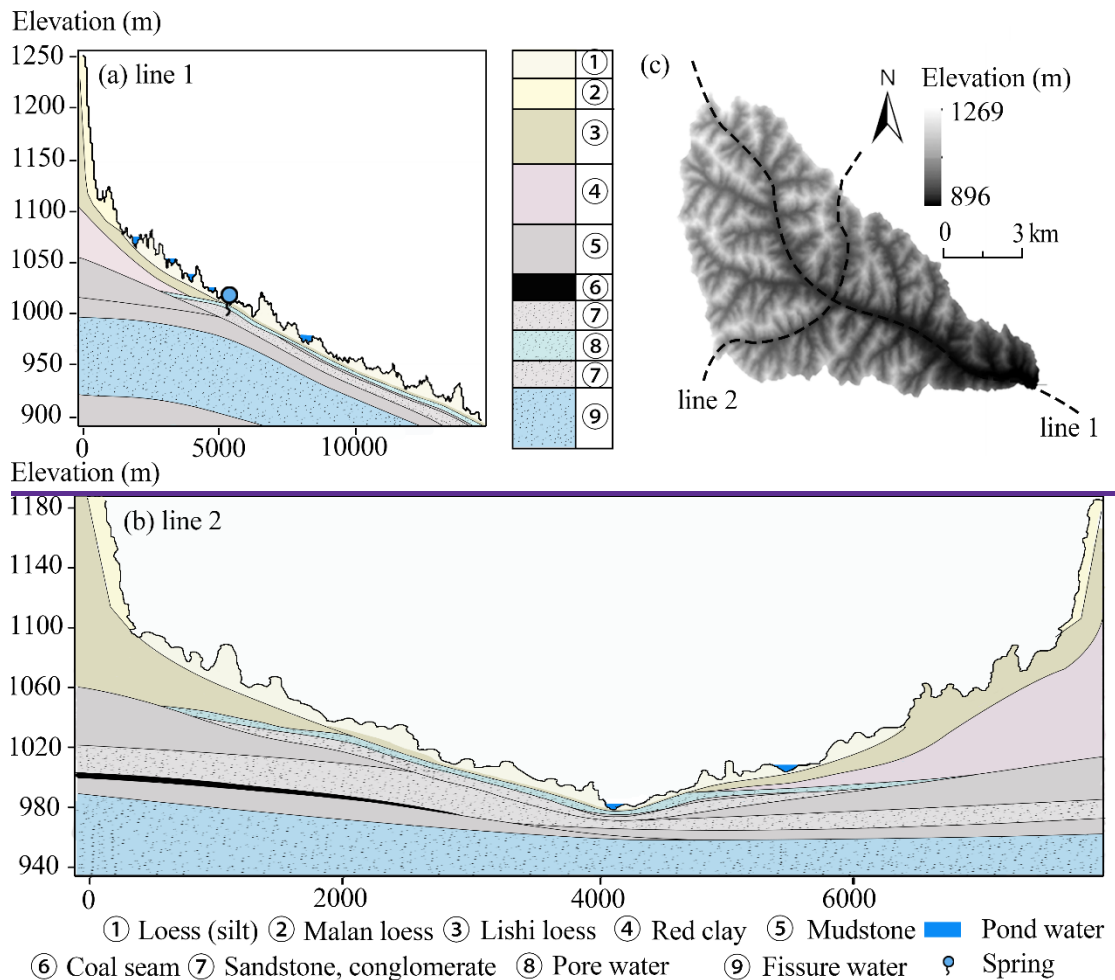
269 Fig. 2. The topographic profile of the Nianzhuang Catchment in the hilly region of the Loess Plateau.
 270 Full profile from the top to mid-slope (a); two repeated mid-slope profiles (b, c). The photo was taken
 271 after a 41 mm rainfall event over four days. Subsequent measurements showed that infiltration depths
 272 reached only 20–30 cm at the top of the slope, compared to approximately 80 cm at the mid-slope
 273 positions.

274

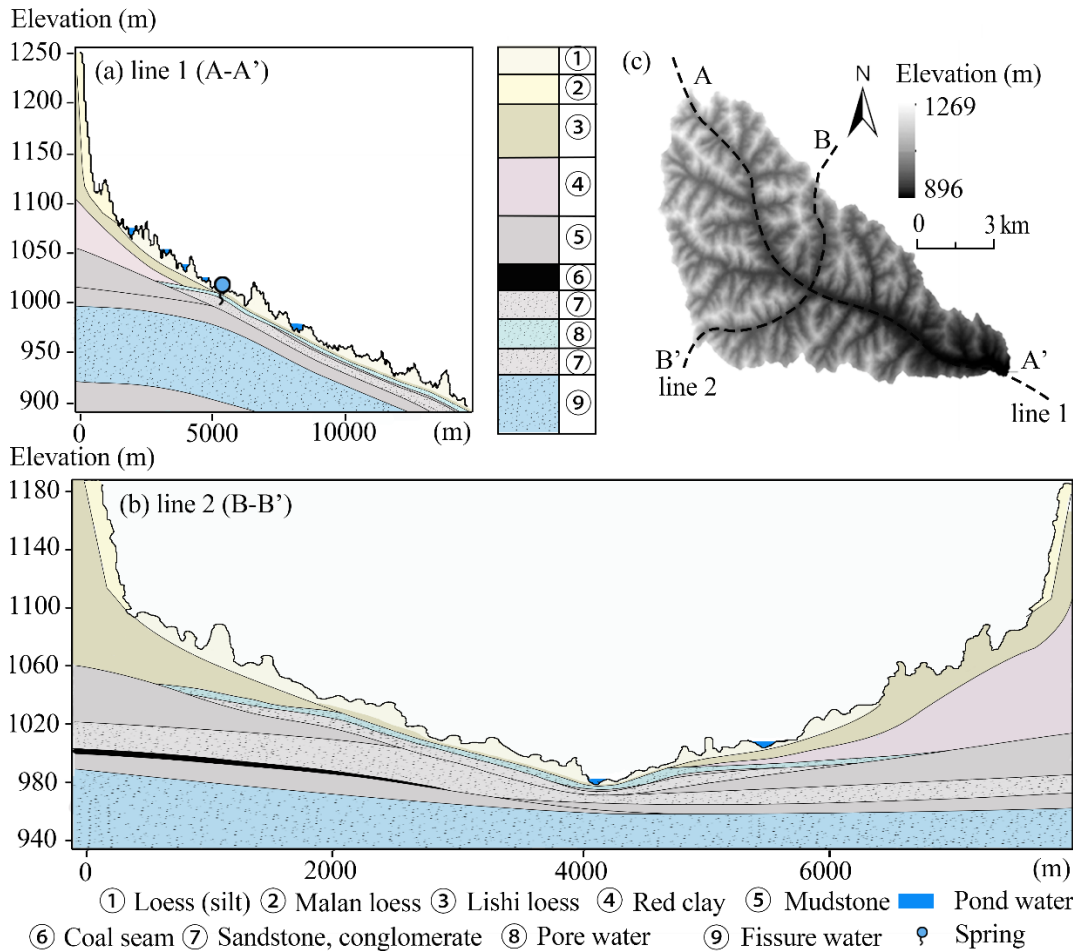
275 The stratigraphy of the catchment reflects the typical layered structure of the Loess Plateau, which
 276 plays a key role in controlling groundwater recharge. In upland hilly areas, thick loess deposits overlie
 277 bedrock, with the Upper Pleistocene Malan Loess—a light grayish-yellow, loosely textured, and silt-
 278 rich unit (>60%)—characterized by well-developed vertical joints and abundant hematite and goethite.
 279 Beneath it lies the Middle Pleistocene Lishi Loess, a grayish-yellow to light brown unit with prominent
 280 jointing and higher iron mineral content. Below the loess, the Neogene Red Clay appears as a distinctly
 281 reddish, calcareous nodule-bearing aquitard due to its low permeability. The entire sequence rests on

282 Jurassic sandstone–conglomerate bedrock, composed mainly of quartz-rich fluvial–lacustrine deposits.

283 Loess thickness in the Liang and Mao regions often exceeds 150 meters, resulting in deep water
 284 tables and limited groundwater accessibility. In contrast, gully zones exhibit distinctly different
 285 hydrogeological characteristics. Here, thinner loess layers overlie Neogene and Jurassic formations,
 286 sometimes interbedded with coal seams up to 5 meters thick (Fig. 3a3a–c). The significant reduction in
 287 loess thickness—, combined with the relatively high permeability of Neogene coarse sandstone and
 288 conglomerate (7.5–36.190.07–0.31 m/d)—, creates favorable conditions for infiltration and focused
 289 recharge. These dynamics are especially evident at gully heads, where surface runoff from adjacent
 290 uplands converges and infiltrates, forming efficient recharge zones. As a result, gully areas tend to have
 291 shallower water tables and more rapid water renewal, making them more suitable for domestic
 292 groundwater use. Springs frequently emerge at gully bottoms where lateral flow is facilitated at the loess–
 293 bedrock interface. Streams in this dry environment are largely intermittent.



294



295

296 Fig. 33. Hydrogeologic cross-section of the study area. Cross-section along Line 1 (Northwest-Southeast)

297 (a); cross-section along Line 2 (Southwest-Northeast) (b); location map of Line 1 and Line 2 within the

298 study area (c). The Malan Loess (11.7–12.6 Ka BP) and Lishi Loess (12.6–78.1 Ka BP) are two major

299 Quaternary loess stratigraphic units in China. Based on hydrogeological research, the stratigraphy of the

300 hilly region features a multi-layer structure from top to bottom: Upper Pleistocene Malan Loess, Middle

301 Pleistocene Lishi Loess, Neogene Red Clay and Mudstone (2.58–23.03 Ma BP), and Jurassic Sandstone

302 and Conglomerate (145–201.3 Ma BP). In the gully region, the stratigraphy includes Holocene loess (silt,

303 11.7 ka BP–present), Middle Pleistocene Lishi Loess, Neogene sandstone and mudstone, and Jurassic

304 sandstone and conglomerate, with some areas containing coal seams up to 5 meters thick.

305

306 Groundwater in the catchment can be broadly categorized into three types: pore water, spring water,

307 and fissure water. Pore water is stored in permeable sandstone and conglomerate aquifers beneath loess

308 and above mudstone or red clay. These aquifers are approximately 2–3 m thick, exhibit a sheet-like

309 distribution, and have low water yield. Conceptually, “pore water” here refers to groundwater in a

310 saturated aquifer, not to soil moisture. Fissure water occurs in fractured bedrock aquifers, which are
311 spatially discontinuous due to irregular fracture development. The main water-bearing zones include
312 cavities and jointed fissure networks, with an average aquifer thickness of about 6 m and moderate water
313 yield. Fissure water occurs within fractured bedrock aquifers but is spatially discontinuous due to
314 irregular fissure development. Hydraulic conductivity in these sandstone and conglomerate aquifers
315 ranges from 0.0218 to 0.474 m/day (Cai et al., 2019). Spring water emerges primarily at gully bases—
316 especially in upper catchments—and originates from both pore and fissure sources, possibly
317 supplemented by surface or pond water. Springs fed by pore water typically have low discharge rates
318 (0 - 0.1 L/s) and low water yield, while those fed by fissure water exhibit moderate discharge rates (0.5 -
319 1.0 L/s) and moderate water yield.

320 Over recent decades, landscape rehabilitation through the Grain for Green Project and land
321 reshaping under the Gully Land Consolidation Project have significantly altered the hydrological regime
322 (Fu et al., 1999; Liu et al., 2017). Historically, surface runoff in the degraded catchment was flashy and
323 episodic due to sparse vegetation. However, ecological restoration and small-scale engineering
324 interventions—such as check dams, terraces, roads, and ponds—have moderated surface hydrology.
325 Surface runoff, generated primarily during storm events, now contributes alongside delayed baseflow
326 from groundwater recharge and interflow. The latter is often limited by the thick unsaturated zone in
327 upland loess areas but may be enhanced in gully regions, where stratigraphy and land use favor
328 infiltration (Wang et al., 2024; Gates et al., 2011). Gully areas also contain numerous check dams and
329 ponds, with most water sourced from Hortonian overland flow of slope lands and direct rainfall. These
330 small water bodies, often constructed for erosion control and water retention, influence local hydrological
331 dynamics and may play a role in enhancing infiltration and recharge.

332

333 **4.3. Methods**

334 Our approach integrates stable isotope analysis ($\delta^2\text{H}$ and $\delta^{18}\text{O}$), chloride concentration analysis, and
335 water table fluctuation monitoring to investigate groundwater recharge dynamics. The isotopic
336 composition of water bodies reflects both their origins and the processes they undergo—such as
337 evaporation, infiltration, and mixing (Wan and Liu, 2016; Kumar et al., 2019; Dasgupta et al., 2024).
338 Precipitation, surface water, and groundwater typically exhibit distinct isotopic signatures due to these

339 differing pathways (Gleeson et al., 2016; Kuang et al., 2019; Al-Oqaili et al., 2020). When isotopic
340 patterns among water sources converge, it often indicates strong hydrological connectivity (Yang and
341 Wang, 2023). Because stable isotopes behave conservatively, they serve as effective tracers of water
342 sources and flow paths (Gleeson et al., 2016; Al-Oqaili et al., 2020; Dasgupta et al., 2024). In parallel,
343 water table fluctuation (WTF) monitoring provides a means of estimating recharge by observing changes
344 in groundwater levels in response to precipitation events (Nachabe, 2002; Heppner and Nimmo, 2005;
345 Gumuła-Kawęcka et al., 2022). By combining these complementary methods, this study aims to elucidate
346 groundwater recharge pathways and quantify recharge rates in gully regions—, thereby identifying key
347 recharge zones and advancing our understanding of groundwater processes in the Loess Plateau.

348

349 **4.3.1. Field measurements of hydrological data**

350 Precipitation was collected from October 24, 2023, to October 24, 2024, using a weather station
351 situated in an open field within the catchment. Continuous groundwater level data were recorded from
352 September 24, 2023, to December 20, 2024. Groundwater pressure and temperature were monitored
353 using Onset HOBO U20-001-03 sensors (20 m range), with a pressure accuracy of $\pm 0.3\%$ FS (± 2.55 kPa)
354 and a resolution of < 0.085 kPa, and a temperature accuracy of ± 0.44 °C with a resolution of 0.1 °C. The
355 sensor was calibrated to atmospheric pressure before installation to ensure accurate measurement of
356 absolute static water pressure, and water table levels were calculated based on the measured pressure
357 data. The conversion relationship between water pressure and groundwater level is given by $Y =$
358 $0.86 \times X - 22.1$ where Y represents the groundwater level and X represents the water pressure. The
359 conversion between water pressure and groundwater level is based on the principle of hydrostatics. The
360 hydrostatic pressure P at the sensor is related to the height of the overlying water column h by $P = \rho gh$,
361 where ρ is the water density and g is the gravitational acceleration. In unconfined aquifer, the pressure
362 measured by the sensor corresponds directly to the static pressure exerted by the overlying water column.
363 From this, the water column height h can be calculated, and combined with the sensor's installation
364 elevation, the depth to the groundwater table can be determined. Notably, the monitoring well is located
365 in the pore water layer of the gully region. The well is hand-dug (1.1 m wide, 10 m deep) and is unaffected
366 by human activities.

367 Soil physical properties were assessed using the cutting ring method, based on undisturbed soil cores
368 collected at five depth intervals: 0–10, 10–20, 20–30, 30–40, and 40–50 cm. Quadruplicate samples were

369 taken near groundwater monitoring wells in the gully using pre-weighed cutting cylinders. The samples
370 were immediately transported to the laboratory for analysis. Bulk density, capillary porosity, non-
371 capillary porosity, total porosity, and field water capacity were determined following the LY/T 1215-
372 1999 standard for forest soil water-physical properties. Soil particle size distribution was analyzed using
373 a laser particle size analyzer at the College of Natural Resources and Environment, Northwest A&F
374 University. Soil texture classification followed the USDA system: sand (0.05–2 mm), silt (0.002–0.05
375 mm), and clay (<0.002 mm) (Dane et al., 2002).

376

377 **4.2 Water sampling**

378 A total of 181 water samples were collected from various locations in rainy season (September 2023,
379 99 samples) and dry season (April 2024, 82 samples); see Fig. 21. Rainy season samples included 48
380 from rainfall, 7 from pond water (water retention reservoirs), 9 from spring water, 9 from pore water, and
381 26 from fissure water. During the dry season, samples included 31 from rainfall, 6 from pond water, 8
382 from pore water, 29 from fissure water, and 8 from spring water.

383 Pore water was collected from several shallow, hand-dug wells measuring approximately 1.1 meters
384 in diameter and 4–10 meters in depth. Fissure water was sampled from deeper, narrow-diameter wells
385 (0.2 meters wide, 25–170 meters deep). In areas with numerous deep wells, we employed random
386 sampling to ensure representative coverage of fissure water sources. To minimize the risk of collecting
387 stagnant water, all pore and fissure water wells were purged for 10–15 minutes prior to sampling. Spring
388 water was collected directly from natural discharge points, although most springs in the region exhibit
389 low flow rates—, typically less than 0.1 L/s, occasionally reaching up to 0.2 L/s.

390 A total of 18 bulk rainfall collectors were randomly and evenly distributed across the 54 km² study
391 area, and samples were collected immediately following rainfall events. For nighttime precipitation,
392 samples were collected the next morning at 6:00 AM. During the study period, we collected two types of
393 precipitation samples: (1) spatial samples from individual events (18 in the rainy season and 15 in the
394 dry season) across the catchment, capturing spatial variability; and (2) sequential events at a fixed station
395 (30 in the rainy season and 16 in the dry season), characterizing seasonal inputs.

396 During sampling, 100 mL collection bottles were rinsed two to three times with the sample water,
397 then slowly filled to minimize air exposure. After filling, the bottles were tightly sealed with screw caps
398 and further secured with Parafilm to prevent evaporation and contamination. All samples were

399 immediately stored in a portable cooler at 4°C and transported to the laboratory for isotopic and chloride
400 concentration analysis.

401

402 **4.3. Isotopic analysis**

403 The $\delta^2\text{H}$ and $\delta^{18}\text{O}$ values of the water samples were determined using a Los Gatos Research liquid
404 water isotope analyzer (Model 912-0032, LGR Inc., California, USA) at the Institute of Water-Saving
405 Agriculture in Arid Areas of China, Northwest A&F University. Each sample was injected six times in
406 the following sequence: three standard injections, followed by six natural sample injections, and then
407 three additional standard injections. The isotope ratios were calculated using the average composition
408 from injections 4 through 6.

409 Isotope values are expressed in delta (δ) notation, which represents the relative difference in isotope
410 ratio between a sample and the Vienna Standard Mean Ocean Water (VSMOW) reference. The
411 measurement precision was $\pm 0.5\text{‰}$ for $\delta^2\text{H}$ and $\pm 0.1\text{‰}$ for $\delta^{18}\text{O}$. The delta values were calculated using
412 the following equations:

$$413 \quad \delta^{18}\text{O} = \left(\frac{R_{\text{sample}}}{R_{\text{standard}}} \right) - 1 \quad (1)$$

$$414 \quad \delta^2\text{H} = \left(\frac{R_{\text{sample}}}{R_{\text{standard}}} \right) - 1 \quad (2)$$

415 where R_{sample} and R_{standard} are the ratios of heavy to light isotopes ($^{18}\text{O}/^{16}\text{O}$ or $^2\text{H}/^1\text{H}$) in the sample
416 and the standard, respectively. Results are expressed in per mil (‰).

417

418 **4.4. Mixing process of different water bodies**

419 Inverse transit time proxies (ITTPs) were calculated to assess differences in water transit times and
420 mixing processes across various water bodies (Tetzlaff et al., 2009). ITTPs are defined as the ratio of the
421 standard deviation of $\delta^{18}\text{O}$ in the water sample (e.g., pond water, spring water, pore water, or fissure
422 water) to that in precipitation over the same time period:

$$423 \quad \text{ITTP} = \frac{\sigma_{\delta^{18}\text{O}}(\text{sample})}{\sigma_{\delta^{18}\text{O}}(\text{precipitation})} \quad (3)$$

424 This ratio captures the attenuation of seasonal isotopic variability in $\delta^{18}\text{O}$ as water moves through
425 the landscape. In general, ITTP values less than 1 indicate substantial damping of the precipitation
426 signal—consistent with longer water residence times, greater mixing, and larger storage volumes.
427 Conversely, values approaching 1 suggest minimal damping and rapid flow paths.

428 However, interpretation of ITTPs must also account for fractionation processes. In particular,
429 evapotranspiration (ET) selectively removes lighter isotopes (^{16}O), enriching the remaining water in
430 heavier isotopes (^{18}O). This enrichment can artificially increase the variance of $\delta^{18}\text{O}$ in near-surface or
431 shallow soil water compartments, inflating ITTP values even in systems with relatively slow transit times
432 (Tetzlaff et al., 2009). This is especially relevant in arid and semi-arid regions, where ET can dominate
433 the water balance during dry seasons.

434

435 **4.5. Hydraulic connectivity estimation**

436 Structural Equation Modeling (SEM) has been widely applied in water science to evaluate complex
437 relationships among hydrological, geological, and anthropogenic variables, particularly in studies of
438 groundwater contamination and water quality degradation (Wu, 2010; Lupi et al., 2019; Xie et al., 2025).
439 In this study, SEM is used explicitly as an exploratory, hypothesis-generating tool to assess potential
440 hydrological connectivity among water sources based on dual-isotope ($\delta^2\text{H}$ – $\delta^{18}\text{O}$) data from rainfall,
441 pond water, spring water, pore water, and fissure water. SEM is not a mass-conserving or process-based
442 flow model, nor is it used here to infer volumetric fluxes, recharge rates, or source apportionment. Instead,
443 it serves as a statistical consistency check on hypothesized connectivity, identifying direct and indirect
444 associations among water bodies that are evaluated in conjunction with tracer evidence and hydrometric
445 observations.~~Structural Equation Modeling (SEM) has been widely applied in water science to evaluate~~
446 ~~complex causal relationships among hydrological, geological, and anthropogenic variables,~~
447 ~~particularly in studies of groundwater contamination and water quality degradation (Wu, 2010; Lupi et~~
448 ~~al., 2019; Xie et al., 2025). In this study, we adapted SEM as an exploratory framework to assess~~
449 ~~hypothesized recharge linkages among water sources, using dual isotope ($\delta^2\text{H}$ – $\delta^{18}\text{O}$) data from rainfall,~~
450 ~~pond water, spring water, pore water, and fissure water. Although SEM is not a mass-conserving approach~~
451 ~~and is less commonly used in isotope based flowpath analysis, it enables estimation of statistically~~
452 ~~significant relationships and indirect linkages within a hypothesized recharge system.~~

453 Within the SEM framework, path relationships are primarily explained through two types of effects:
454 The direct effect refers to the immediate impact of one variable on another through a single path, typically
455 quantified as a standardized regression coefficient. Total effect represents the overall impact of one
456 variable on another through all possible paths (including both direct and indirect), calculated as the sum
457 of the direct effect and all indirect effects. Comparing direct and total effects allows identification of

458 intermediary linkages and dominant association structures within the hypothesized connectivity network.
459 ~~Interpreted cautiously and in combination with independent indicators, these results provide quantitative~~
460 ~~support for relative connectivity patterns, rather than definitive evidence of causal flow paths or recharge~~
461 ~~magnitudes. By comparing the direct and total effects, the complex causal network and interaction~~
462 ~~strength between variables can be systematically revealed, providing a quantitative basis for~~
463 ~~understanding hydrological processes.~~

464 Given the potential for isotopic signatures to be altered by evaporation, mixing, or other non-
465 conservative processes, results must be interpreted with caution. Pathways with p-values > 0.05 were
466 excluded during model refinement, and the final model met standard goodness-of-fit criteria (degrees of
467 freedom < 3, RMSEA < 0.05, CFI > 0.95, NFI > 0.95). SEM analysis was conducted using SPSS Amos
468 26.0 (IBM SPSS, Chicago, Illinois, USA).

469 In addition, we applied variance partitioning to evaluate the relative contributions of different water
470 sources to pore and fissure water. This method decomposes the total variance in isotopic composition
471 into components attributable to individual sources (e.g., precipitation, pond water, spring water), offering
472 a complementary estimate of source influence. While useful, this approach remains subject to the same
473 limitations as SEM—, particularly the challenges of isotopic overlap and limited resolution in
474 environments affected by mixing and evaporation (Lai et al., 2022).~~While useful, this approach remains~~
475 ~~subject to the same limitations as SEM—particularly the challenges of isotopic overlap and limited~~
476 ~~resolution in environments affected by mixing and evaporation (Lai et al., 2022).~~

477 To further constrain recharge pathways, we incorporated chloride ion (Cl⁻) as a conservative tracer.
478 Unlike stable isotopes, Cl⁻ behaves conservatively with respect to fractionation, but its concentration can
479 increase under evaporation and decrease under dilution; and when interpreted alongside isotopes, it can
480 still constrain further explain mixing and recharge pathways~~chloride is unaffected by evaporation or~~
481 ~~biological processes, making it a robust indicator for identifying recharge sources and tracking~~
482 ~~subsurface water movement.~~ Chloride concentrations in all water samples were analyzed using an ion
483 chromatograph (DIONEX ICS-1100) at the College of Natural Resources and Environment, Northwest
484 A&F University, China. Each sample was analyzed in triplicate, with charge balance errors maintained
485 below 5% to ensure analytical accuracy. This rigorous approach enhances the reliability of chloride data,
486 supporting its integration with isotopic indicators in source attribution.

487

488 **4.3.6. Groundwater recharge**

489 Groundwater recharge in the gully zone is quantified using the water table fluctuation (WTF)
490 method, which infers recharge and discharge events from temporal changes in groundwater levels (Healy
491 and Cook, 2002; Gumuła-Kawęcka et al., 2022). We recognize that recharge can originate from three
492 hydrological sources: (1) surface water; (2) the unsaturated zone (3) and the saturated zone (Scanlon et
493 al., 2022; Wang et al., 2024). Among these, estimates based on the saturated zone are generally most
494 reliable, as recharge from the unsaturated zone reflects potential inputs that may never reach the water
495 table (Beven and Germann, 2013; Huang et al., 2019). The WTF method is widely used for estimating
496 saturated zone recharge due to its high temporal resolution and conceptual simplicity (Xu et al., 2024).
497 Based on previous site-specific studies (Wang et al., 2024), this method is well-suited for our analysis.

498 The water table fluctuation method assumes that changes in the groundwater table result solely from
499 recharge or discharge, assuming a constant specific yield (S_y) over time (Healy and Cook, 2002; Obuobie
500 et al., 2012). The formula is as follows:

$$501 \quad R_i = S_y \frac{\Delta H_i}{\Delta t} \quad (4)$$

502 where, R is the groundwater recharge (mm), S_y is the specific yield of the aquifer, ΔH_i (where
503 $\Delta H_i > 0$) is ~~the groundwater table rise in groundwater level e caused by recharge~~ between days $i -$
504 1 and i , and Δt is ~~the time interval (one day) is time period~~. Specific yield, which ~~represents effective~~
505 ~~drainable porosity of the shallow gully aquifer system~~ ~~represents the proportion of water that drains freely~~
506 ~~from the saturated zone under gravity , rather than soil water release from the unsaturated zone. In this~~
507 ~~study, S_y was determined-estimated~~ using two ~~complementary approaches: (1) an empirical method~~
508 ~~based on soil texture to constrain plausible ranges of drainable porosity, and (2) the test pit method, in~~
509 ~~which S_y is calculated as the difference between total porosity and field water capacity (Liang, 2016).~~
510 ~~These approaches provide an estimate of aquifer-scale effective specific yield appropriate for shallow~~
511 ~~unconfined groundwater systems in loess-derived gully environments. methods: the soil texture empirical~~
512 ~~method and the test pit method (Liang, 2016).~~

513 Empirical values for soil texture are referenced in Table A1. The test pit method for estimating S_y is
514 described as follows:

$$515 \quad S_y = TP - FWC \quad (5)$$

516 where, TP (total porosity) and FWC (field water capacity) were measured using the cutting ring

517 method.

518 We applied two methods to calculate the daily groundwater table increments (ΔH_i). The RISE
519 method assumes that recharge occurs only when the groundwater table elevation increases between two
520 consecutive days (Gumuła-Kawęcka et al., 2022). Thus, $\Delta H_i = H_i - H_{i-1}$ if $H_i > H_{i-1}$, otherwise,
521 $\Delta H_i = 0$. The master recession curve (MRC) method assumes that, in the absence of recharge, the
522 groundwater table declines daily by a specific amount (ΔH_{MRCi}). This amount represents a simplified
523 approximation of discharge processes in the aquifer, particularly lateral outflow to nearby surface water
524 bodies. MRC establishes a functional relationship between a daily decrement of the water table (ΔH_{MRCi})
525 and the water table elevation (H_{i-1}) during periods without recharge.

$$526 \quad \Delta H_{MRCi} = A \cdot H_{i-1} + B \quad (6)$$

527 where, the coefficients A and B were fitted for each piezometer based on data from periods of
528 continuous groundwater table decreases lasting longer than two weeks. The daily water table increment
529 due to recharge was then calculated as: $\Delta H_i = H_i - H_{i-1} + \Delta H_{MRCi}$ if $H_i > (H_{i-1} - \Delta H_{MRCi})$,
530 otherwise, $\Delta H = 0$.

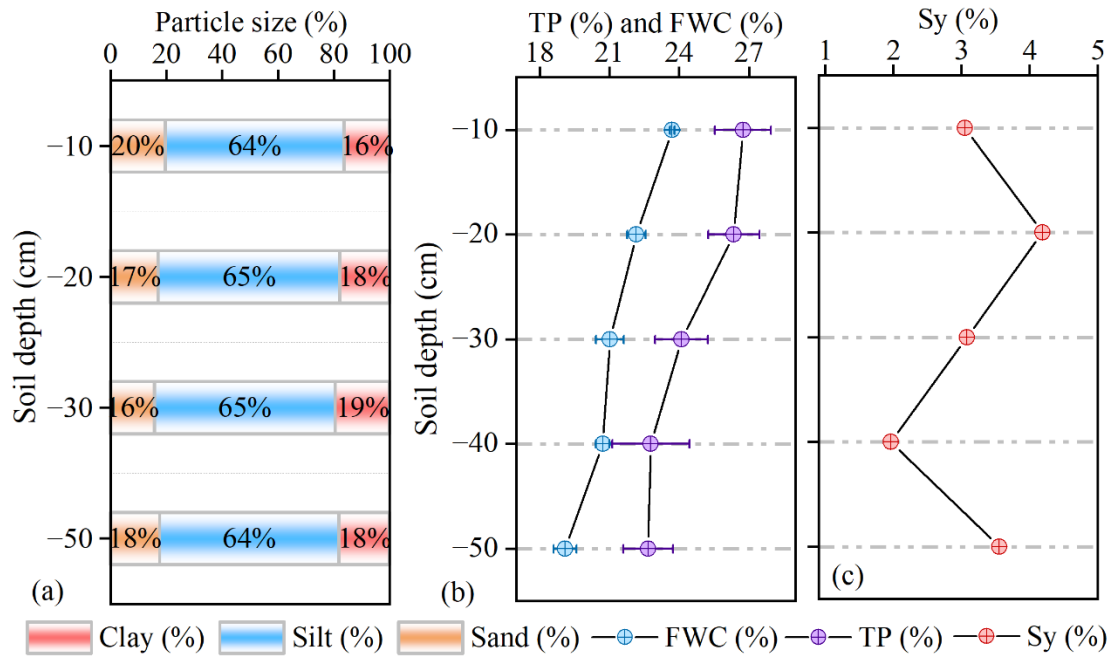
531 Notably, we used water dynamics from October 24, 2023, to October 24, 2024, to calculate pore
532 water recharge, as this period exhibited clear groundwater fluctuations, making it more representative.

533

534 **5.4. Results**

535 **5.4.1. Soil properties**

536 The upper 50 cm of the soil profile is composed primarily of silt ($64.6 \pm 0.6\%$), with smaller but
537 nearly equal proportions of clay ($18.0 \pm 1.3\%$) and sand ($17.4 \pm 1.6\%$), classifying the loess as silt loam
538 according to the International Union of Soil Sciences (IUSS) scheme (Fig. 4a). Total porosity and field
539 water capacity decreased slightly with depth, averaging $24.5 \pm 1.9\%$ and $21.3 \pm 1.7\%$, respectively (Fig.
540 4b). Specific yield remained relatively consistent within the 10–50 cm depth interval, averaging
541 $3.2 \pm 0.8\%$, falling within the expected empirical range for silt loam soils (2%–7%) (Fig. 4c).

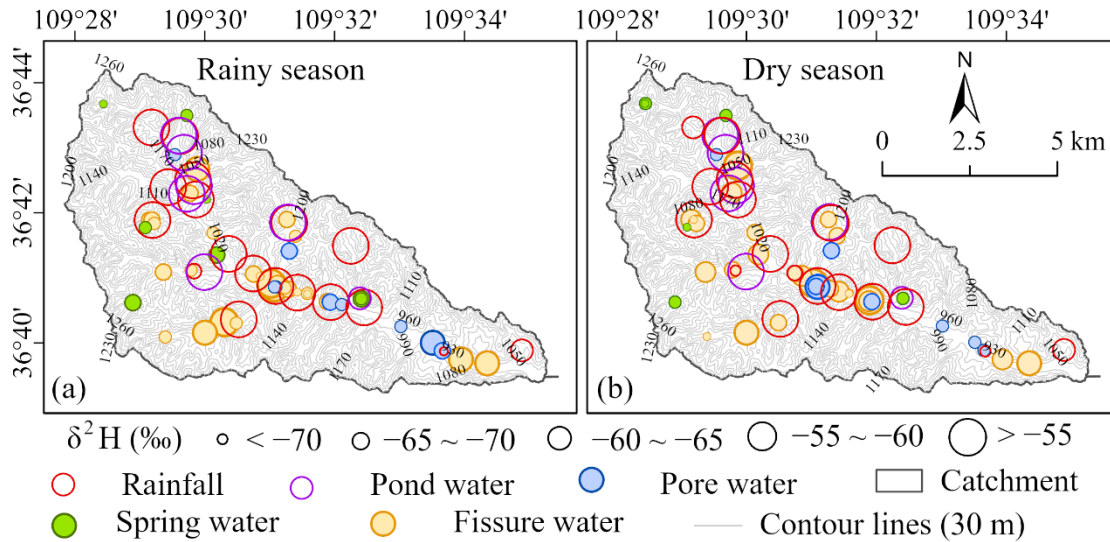


542
 543 Fig. 4. Vertical variation in soil texture and water retention characteristics in the gully region of the Loess
 544 Plateau. (a) Soil particle size distribution by depth, showing relatively uniform composition across layers
 545 (10–50 cm), dominated by silt (64–65%), with moderate clay (16–20%) and low sand (16–20%) content.
 546 This fine-textured profile supports high moisture retention and slows infiltration, promoting delayed
 547 recharge. (b) Depth profiles of total porosity (TP) and field water capacity (FWC) reveal ~~increases~~
 548 ~~decreases~~ with depth to 40 cm, with FWC reaching ~27%, suggesting greater water-holding capacity in
 549 subsoil layers and enhanced buffering of infiltrated water. (c) ~~Vertical variations in the Specific Yield~~
 550 ~~(Sy) across different soil layers. Specific yield (Sy) peaks at -20 cm (4.5%) but decreases with depth,~~
 551 ~~indicating shallower layers are more responsive to infiltration and release, while deeper layers tend to~~
 552 ~~store water with minimal drainage.~~ Collectively, these physical properties reflect a vertically stratified
 553 soil system where near-surface layers regulate infiltration pulses, and deeper layers act as long-term
 554 storage, shaping the timing and magnitude of subsurface recharge.

555

556 **5.4.2. Hydrological signatures of rainfall, surface water, and groundwater sources**

557 Pond water and rainfall exhibit similar spatial isotopic patterns, with more positive $\delta^2\text{H}$ values ($\delta^2\text{H} >$
 558 -55‰) than spring water, pore water, and fissure water (Fig. 5a, b). These values are line with the notion
 559 of direct rainfall and Hortonian runoff are the primary source of pond water. In contrast, the $\delta^2\text{H}$ values
 560 of pore, spring, and fissure water show little seasonal variation and are consistently more negative ($\delta^2\text{H}$
 561 $< -55\text{‰}$), than mean rainfall, indicating longer residence times and reduced evaporative influence.



562

563

564

565

566

567

568

569

570

571

572

573

574

575

576

577

578

579

580

581

582

583

Fig. 5. The spatial distributions of $\delta^2\text{H}$ values during the (a) rainy season and (b) dry season for rainfall, pond water, spring, pore water, and fissure water in the gully region of the Loess Plateau. To highlight spatial differences among water sources, $\delta^2\text{H}$ values were classified into five intervals: $< -70\text{‰}$, -70 to -65‰ , -65 to -60‰ , -60 to -55‰ , and $> -55\text{‰}$. Sampling points are color-coded by water type: red for rainfall, purple for pond water, blue for pore water, green for spring water, and orange for fissure water.

The $\delta^2\text{H}$ - $\delta^{18}\text{O}$ relationships and box plots for each water source reveal key insights into the dominant hydrological processes occurring during the rainy season (Fig. 6). Firstly, rainfall follows a Local Meteoric Water Line (LMWL) of $\delta^2\text{H} = 7.7 \cdot \delta^{18}\text{O} + 8.9$ ($R^2 = 0.95$), which is closely aligned— though slightly offset— from the Global Meteoric Water Line (GMWL: $\delta^2\text{H} = 8 \cdot \delta^{18}\text{O} + 10$) (rainy season; Fig. 6a, c). This alignment indicates that precipitation in the region has a typical meteoric origin. Additionally, minimal evaporative enrichment occurred prior to collection. The relatively wide interquartile range of rainfall $\delta^{18}\text{O}$ values suggests that precipitation was derived from storm systems with considerable isotopic variability, reflecting differences in rainfall intensity, air mass origin, and temperature (Kumar et al., 2019; Oqaili et al., 2020; Dasgupta et al., 2024). However, this variability remains moderate compared with global patterns that span extreme rainfall events and broader climatic gradients.

Pond water, in contrast, exhibits a clear evaporation signature with a shallower slope of $\delta^2\text{H} = 5.6 \cdot \delta^{18}\text{O} - 17.1$ (rainy season; $R^2 = 0.95$), $\delta^2\text{H} = 4.6 \cdot \delta^{18}\text{O} - 20.7$ (dry season; $R^2 = 0.74$). This signature aligns with expectations for surface water bodies, where open exposure facilitates fractionation. The box

584 plot shows strong evaporative enrichment, with median values shifted significantly toward more positive
585 $\delta^{18}\text{O}$ and $\delta^2\text{H}$ compared to rainfall (Fig. 6a, c). Pond water maintains a relatively consistent slope and
586 range across seasons, reinforcing its stable evaporative signature and less dynamic recharge behavior.

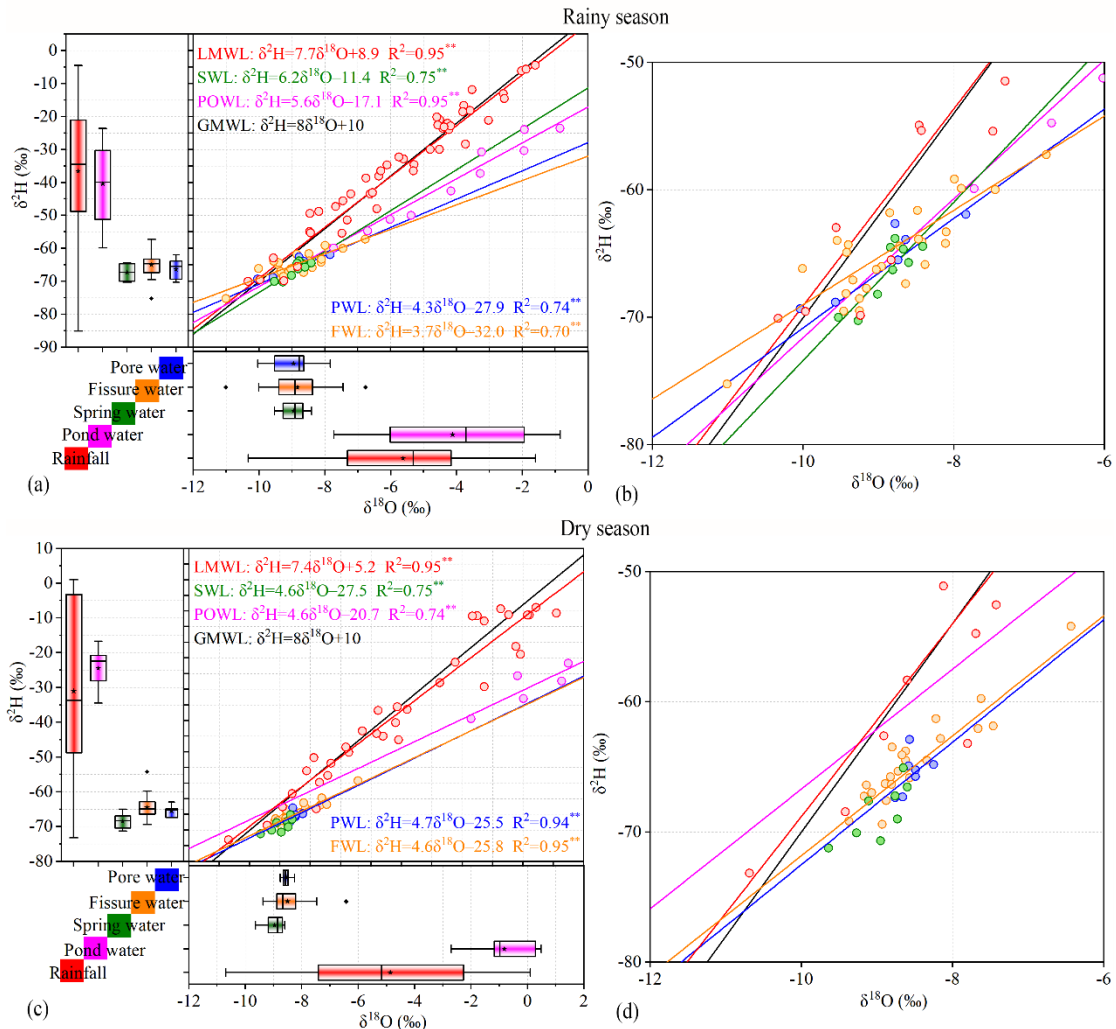
587 Spring water shows a clear seasonal transition in its isotopic composition. In the rainy season, its
588 evaporation line ($\delta^2\text{H} = 6.2 \cdot \delta^{18}\text{O} - 11.4$; $R^2 = 0.75$) falls closer to the LMWL, suggesting that spring
589 discharge is augmented by recent rainfall, likely delivered through rapid infiltration and shallow
590 subsurface flow pathways during high-intensity events (Fig. 6a, b). However, the isotopic values of
591 spring water are substantially more depleted than those of precipitation, indicating that older water stored
592 in the porous subsurface aquifer dominates the overall spring flow composition composed of new and
593 relatively old water.

594 During the dry season, the isotopic slope flattens and deviates further from the Local Meteoric Water
595 Line (LMWL), reflecting increased evaporative influence or prolonged residence times (Fig. 6c, d). This
596 seasonal shift suggests that as rainfall inputs decline, spring discharge becomes increasingly composed
597 of slow-draining, older water that has undergone greater isotopic modification—, either through mixing
598 or evaporation in near-surface storage zones. Collectively, these patterns suggest that spring water acts
599 as a dynamic integrator of recharge processes—, rapidly responding to event-driven infiltration during
600 the rainy season, yet also reflecting the delayed mobilization of older water stored in the subsurface. This
601 behavior may be partly explained by a piston-like displacement mechanism, where incoming rainfall
602 pushes pre-existing groundwater toward discharge zones.

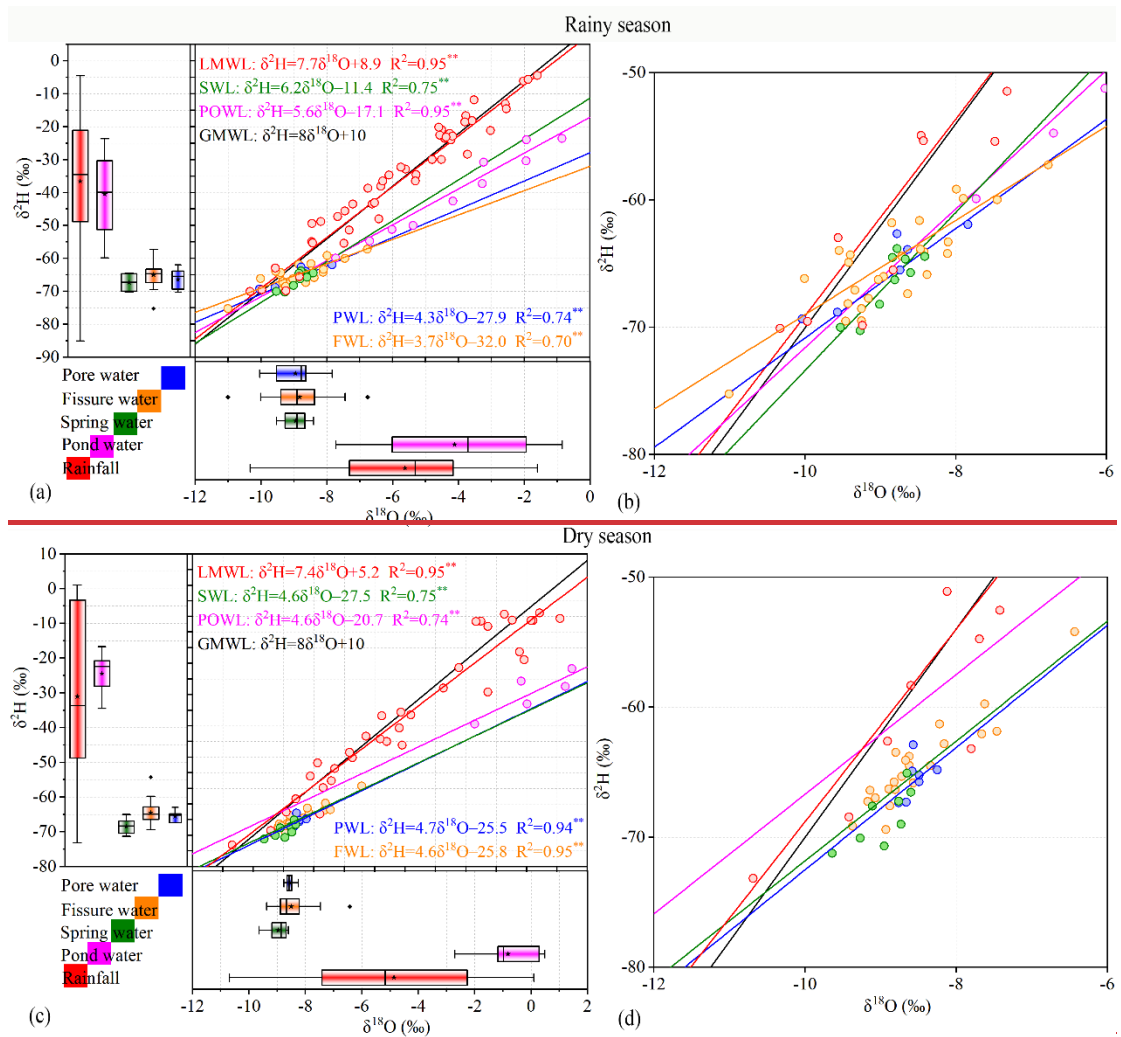
603 Pore and fissure water show remarkably similar isotopic signatures during the rainy season. Pore
604 water, again sampled from a porous subsurface aquifer, follows a fitted line of $\delta^2\text{H} = 4.3 \cdot \delta^{18}\text{O} - 27.9$
605 (rainy season; $R^2 = 0.74$), while fissure water, likely drawing from the same aquifer but through
606 weathered bedrock pathways, fits $\delta^2\text{H} = 3.7 \cdot \delta^{18}\text{O} - 32.0$ (rainy season; $R^2 = 0.70$). These slopes are
607 significantly flatter than those of rainfall, pond, or spring water, a pattern interpreted as evidence of
608 evaporation prior to recharge or mixing with evaporated surface water. However, the box plots of the
609 isotope data present a different picture. Both pore and fissure waters are systematically more depleted in
610 $\delta^{18}\text{O}$ and $\delta^2\text{H}$ than precipitation, and their narrow interquartile ranges suggest a relatively uniform
611 isotopic composition (Fig. 6a-d).

612 [These depleted and uniform isotopic compositions indicate recharge dominated by isotopically light](#)
613 [rainfall events—, primarily intense summer monsoon storms—, rather than evaporative enrichment.](#)

614 [Depleted groundwater signatures thus reflect recharge from these summer events, with percolation](#)
 615 [delayed to cooler seasons due to soil storage and reduced evaporation. The flat regression slopes and](#)
 616 [narrow interquartile ranges are reconciled by longer residence times and mixing in the subsurface aquifer,](#)
 617 [which acts as a hydrological buffer that dampens seasonal isotopic variability \(Table A2\).](#)



618
 619 [Rather than showing the enrichment expected from evaporation, these depleted and stable values point](#)
 620 [toward recharge dominated by a limited number of isotopically light rainfall events, such as early-season](#)
 621 [storms or high-altitude convective systems.](#)



622

623

Fig. 6. Dual stable isotopic compositions of rainfall, pond water, spring water, pore water, and fissure water during the (a) rainy season and (b) dry season in the gully region of the Loess Plateau. The black line represents the global meteoric water line (GMWL, $\delta^2\text{H}=10 + 8\delta^{18}\text{O}$). GMWL is the global meteoric water line of Craig, LMWL is the local meteoric water line, SWL is the spring water line, POWL is the pond water line, FWL is the fissure water line, and PWL is the pore water line. Panels (b) and (d) are magnified views of (a) and (c), respectively, highlighting the isotopic compositions of pore water, fissure water, and spring water (x-axis: -12 to -6‰ ; y-axis: -80 to -50‰).

630

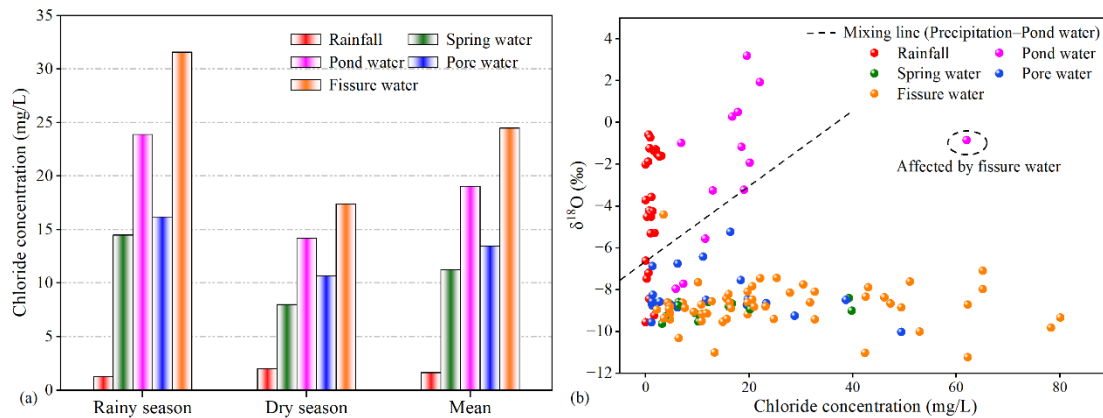
631

~~This apparent contradiction—flat regression slopes alongside depleted and uniform isotopic compositions—can be reconciled by considering longer residence times and mixing in the subsurface. The aquifer likely functions as a hydrological buffer, smoothing short term isotopic variability and maintaining a signature reflective of older recharge. In this context, the low slopes may not indicate evaporation but instead reflect the dampening of seasonal isotope fluctuations through storage and~~

635

636 subsurface mixing (Table A2).

637 ~~Complimenting-Complementing~~ the isotope data, Cl^- levels in pore water consistently fall between
638 those of precipitation and pond water across both seasons (Fig. A27a), ~~and the correlation pattern~~
639 ~~between chloride concentration and $\delta^{18}\text{O}$ supporting supports~~ a mixed recharge origin for pore water (Fig.
640 7b). This trend aligns with the isotopic evidence from the rainy season and supports the interpretation
641 that pond water contributes to pore water recharge via vertical percolation through the vadose zone,
642 particularly during high-rainfall periods when infiltration capacity is exceeded. ~~The lack of a similar~~
643 ~~isotopic pattern in the dry season likely reflects stronger evaporative enrichment of pond water, which~~
644 ~~masks its potential contribution to pore water recharge in dual-isotope space.~~

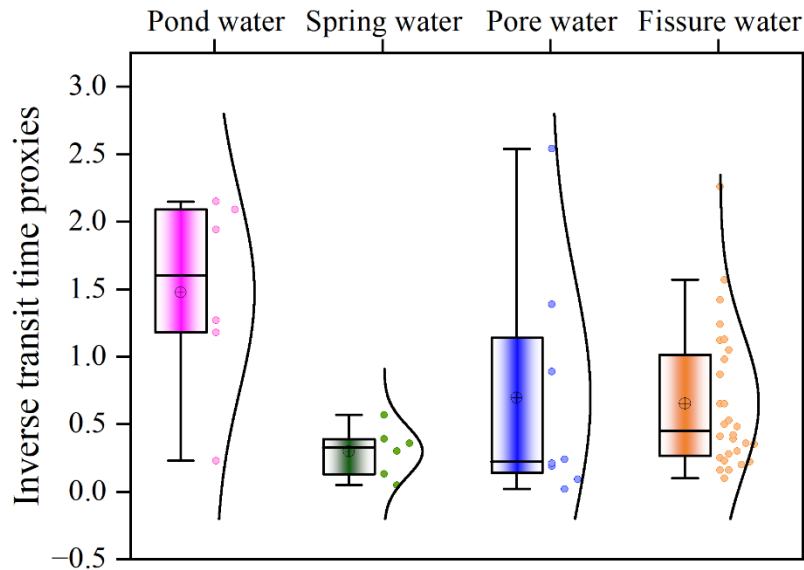


645 (a) Rainy season Dry season Mean (b) Chloride concentration (mg/L) $\delta^{18}\text{O}$ (‰)

646 Fig. 7. Chloride concentration of various water sources in the rainy and dry seasons (a), and the spatial
647 relationship between chloride concentration and $\delta^{18}\text{O}$ for different water sources (b).

648

649 The inverse transit time proxies (ITTPs) broadly support the dual-isotope interpretations of water
650 source dynamics. Pond water exhibited the highest ITTP values (1.5 ± 0.7), indicating rapid turnover and
651 limited subsurface storage. These elevated values likely reflect inputs from direct rainfall and overland
652 flow, as well as evaporative enrichment, which increases isotopic variability and can artificially shorten
653 the apparent residence time. In contrast, pore water (0.7 ± 0.3) and fissure water (0.6 ± 0.5) showed lower
654 ITTPs, consistent with longer residence times, greater subsurface mixing, and attenuation of seasonal
655 isotopic signals due to delayed recharge. Spring water had the lowest ITTPs (0.3 ± 0.2), reflecting slow
656 subsurface transport and integration of older water sources. ~~While these patterns align with conceptual~~
657 ~~expectations of residence time and flow path length, the limited number of samples—particularly for~~
658 ~~pond, spring, and pore water—warrants caution in interpreting seasonal dynamics (Fig. 7.8).~~



659

660 Fig. 78. Boxplots and kernel density estimates of inverse transit time proxies (ITTPs) for pond water,
 661 spring water, pore water, and fissure water. Higher ITTP values indicate shorter water transit times since
 662 precipitation, while lower values suggest longer residence and greater isotopic damping. Pond water
 663 exhibited the highest and most consistent ITTPs (median ≈ 1.5), implying rapid recharge from recent
 664 rainfall or stormflow. Spring water showed the lowest ITTPs (≈ 0.3), consistent with longer subsurface
 665 flow paths and storage. Pore and fissure water displayed intermediate and more variable ITTPs, reflecting
 666 mixing between recent and older water sources, as well as seasonal differences in infiltration and soil
 667 moisture replenishment.

668

669 54.3. Hydrological linkages and recharge efficiency site-scale recharge

670 The SEM analysis reveals significant hydrological linkages among different water bodies in the
 671 catchment, with particularly well-defined pathways connecting rainfall, pond water, pore water, and
 672 fissure water (Fig. 8a 9a, b). ~~Several key pathways identified in the model are supported by multiple lines
 673 of observational evidence, including isotopic composition, chloride concentrations, and water age (ITTP).~~
 674 Rainfall contributes over 73% to pore water recharge, far exceeding the <17% contribution from pond
 675 water (Fig. 8e9c).

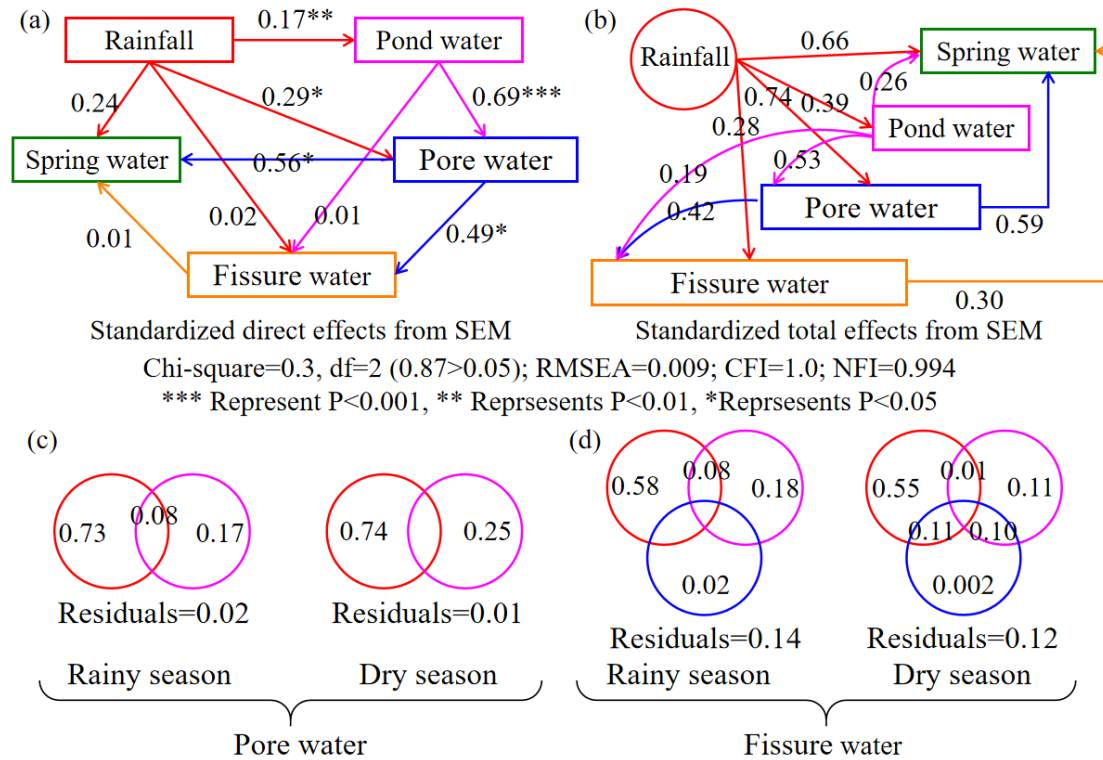
676 However, the SEM results indicate that the total-direct effect of pond water on pore water is stronger
 677 than that of rainfall (Fig. 8b 9b). ~~In SEM, the total effect includes both direct pathways (e.g., pond water
 678 \rightarrow pore water) and indirect pathways mediated by other variables (e.g., rainfall \rightarrow pond water \rightarrow pore
 679 water).~~ This apparent contradiction likely stems from the strong statistical association between rainfall

680 and pond water, as pond water is primarily derived from rainfall and shares similar isotopic signatures.
681 ~~As a result, the model may overestimate pond water's influence on pore water due to overlapping signals~~
682 ~~and correlated pathways.~~

683 These findings underscore the importance of integrating multiple lines of evidence rather than
684 relying solely on SEM outputs. For example, chloride concentrations in pore water more closely resemble
685 those of pond water, suggesting that pond water may contribute to pore water recharge under specific
686 spatial or temporal conditions (Fig. 7a). The spatial distributions of chloride concentration and $\delta^{18}\text{O}$
687 further show that part of the pore water plots near the precipitation–pond water mixing line, providing
688 evidence that pond water can contribute to pore water recharge, particularly in localized areas or during
689 discrete recharge events (Fig. 7b). ~~suggesting mixed recharge from both sources and highlighting the~~
690 ~~potential for pond water to play a prominent role under certain spatial or temporal conditions (Fig. 2a).~~
691 ~~Although dry season isotopic data provide limited support for a strong pond water–pore water connection,~~
692 ~~the spatial distribution of chloride offers compelling evidence that pond water can contribute significantly~~
693 ~~to pore water recharge, particularly in localized areas or during specific recharge events.~~

694 At deeper levels, the linkage between pore water and fissure water is supported by their nearly
695 identical isotope values and similar ITTPs, suggesting a shared subsurface origin and a strong
696 hydrological connection (Fig. 8a9a, b). In contrast, although there is some hydrological connectivity
697 between pore water and spring water, differences in isotopic slopes and residence times may lead to an
698 overestimation of their interaction. However, their nearly identical spatial distributions of chloride
699 concentrations and $\delta^{18}\text{O}$ -chloride concentrations provide more direct and reliable evidence of connectivity.

700 ~~Although the model results initially suggest that rainfall—mediated through pond water—is the~~
701 ~~primary source of pore water recharge, discrepancies among the different indicators call for a more~~
702 ~~critical interpretation of the evidence. The contradictions observed across isotopic, chloride, and ITTP~~
703 ~~data underscore the need for further quantitative validation.~~



704

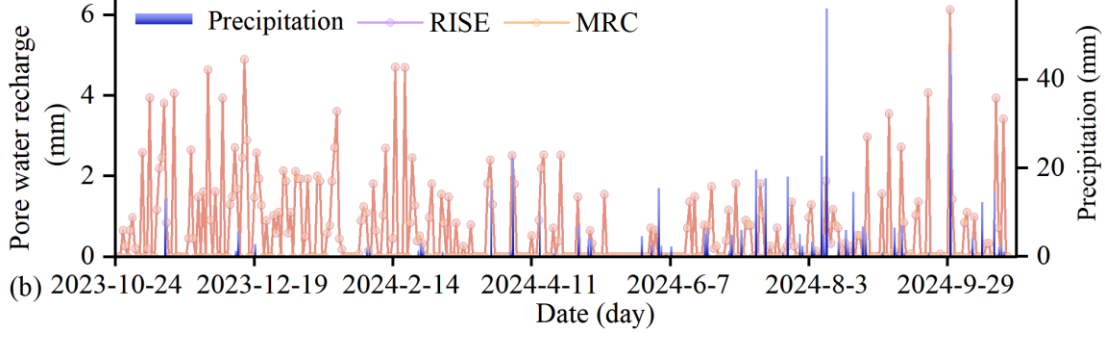
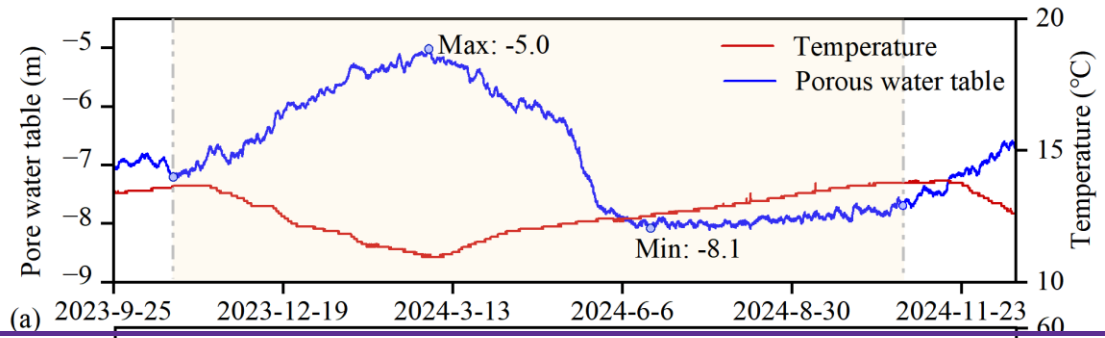
705 Fig. 89. Structural equation modeling (SEM) and variance partitioning results illustrating hydraulic
 706 connectivity among water sources in the gully region of the Loess Plateau. Panels (a) and (b) show the
 707 standardized direct (a) and total effects (b) among rainfall, pond water, pore water, spring water, and
 708 fissure water, based on $\delta^{18}\text{O}$ and $\delta^2\text{H}$ data. In SEM, the total effect includes both direct pathways (a; e.g.,
 709 rainfall \rightarrow pore water) and indirect pathways mediated by other variables (b; e.g., rainfall \rightarrow pond water
 710 \rightarrow pore water). Arrows indicate hypothesized water flow pathways, with line thickness proportional to
 711 effect size. Asterisks denote statistical significance (*P < 0.05, **P < 0.01, ***P < 0.001). The model fit
 712 is excellent ($\chi^2 = 0.3$, df = 2, RMSEA = 0.009, CFI = 1.0, NFI = 0.994), supporting the robustness of these
 713 inferred connections. Panels (c) and (d) present variance partitioning results showing the relative
 714 contributions of source waters to pore water and fissure water during the rainy and dry seasons,
 715 respectively. In panel (c), rainfall (red) and pond water (pink) explain a large portion of pore water
 716 variability, with some shared explanatory power and modest residuals. In panel (d), fissure water reflects
 717 a more complex origin, with contributions from rainfall (red), pond water (pink), and pore water (blue),
 718 and greater overlap and residuals, especially during the dry season.

719

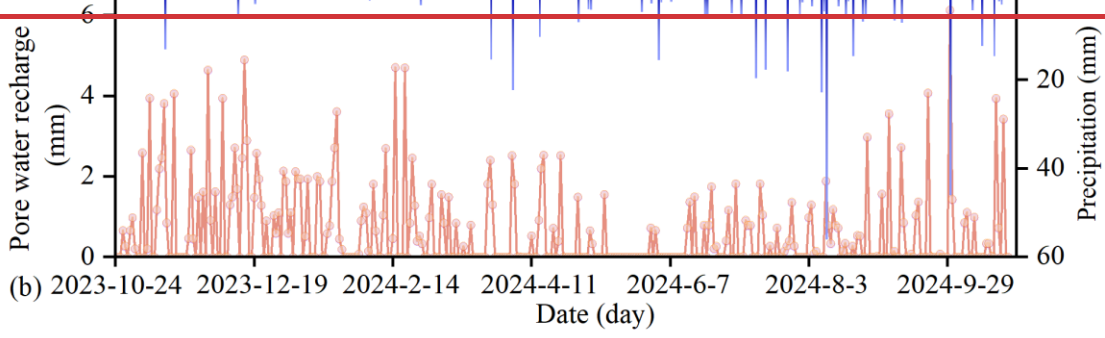
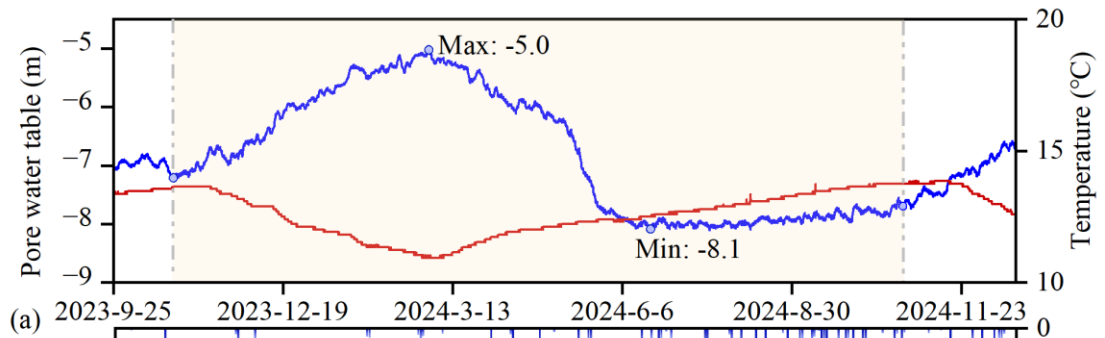
720 Although the model results initially suggest that rainfall, mediated through pond water, is the
 721 primary source of pore water recharge, discrepancies among the different indicators call for a more

722 critical interpretation of the evidence. The contradictions observed across isotopic, chloride, and ITTP
723 data underscore the need for further quantitative validation. To address the contradictions observed in the
724 SEM and variance partitioning results, we apply the water table fluctuation method to independently
725 estimate the recharge rate from rainfall to pore water. Groundwater level fluctuations in the gully system
726 revealed clear seasonal recharge dynamics, with an initial rise in the pore water table beginning on
727 October 24, 2023, followed by a decline through early spring (March 1, 2024) and a gradual recovery
728 starting June 20, 2024 (Fig. [9a10a](#)). Between October 24, 2023, and October 24, 2024, cumulative
729 recharge was estimated at 238.0 ± 6.0 mm (RISE) and 241.4 ± 6.0 mm (MRC), with 159 and 167 recharge
730 days, respectively (Fig. [9b10b, c](#)). Given that annual precipitation totaled approximately 550 mm,
731 “~~recharge efficiency~~site-scale” recharge was approximately 43–44%, underscoring the significance of
732 focused infiltration in sustaining shallow aquifer recharge within the gully environment.

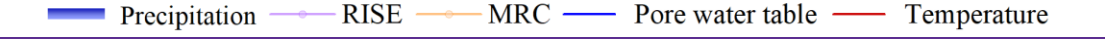
733 This Site-scale recharge efficiency is lower than the precipitation-to-pore water contribution
734 estimated by the variance decomposition method and may more accurately reflect “actual” recharge, as
735 statistical estimates can be biased by similarities in isotopic signatures. Combined with dual-isotope and
736 SEM analyses, the WTF results support a conceptual model where storm runoff is captured and
737 redistributed through loess soils and retention structures, enabling both shallow and deeper subsurface
738 flow. ~~When integrated with dual isotope and SEM analyses, the WTF based results support a conceptual~~
739 ~~model in which storm driven runoff is efficiently captured and redistributed through loess soil matrices~~
740 ~~and retention structures (e.g., ponds, check dams), activating a hierarchy of shallow and deeper~~
741 ~~subsurface flowpaths.~~ These flow paths link pore water, fissure water, and spring discharge across the
742 complex gully landscape, reflecting both vertical and lateral connectivity within the groundwater system.

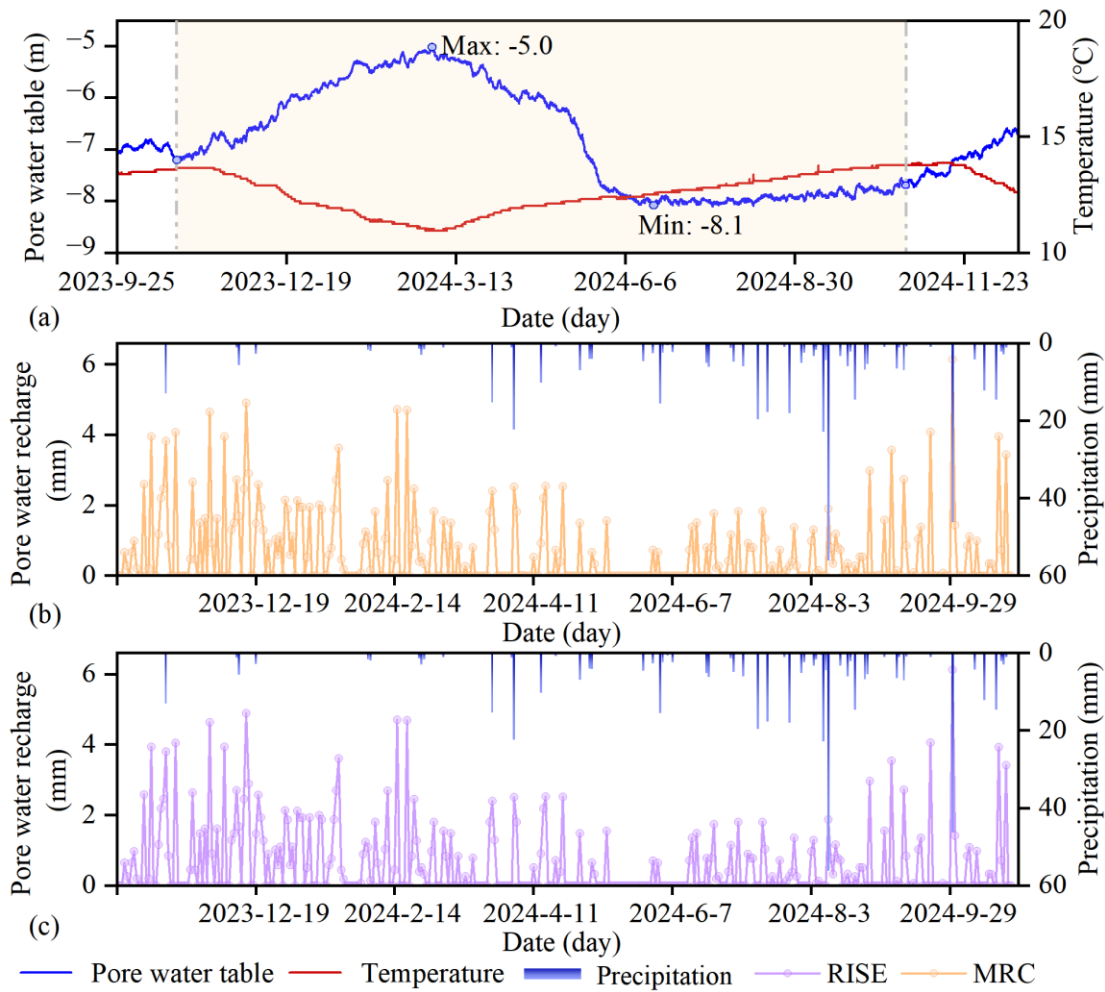


743



744





745

746 Fig. 910. Temporal dynamics of pore water table depth, temperature, precipitation, and recharge in the
 747 gully region of the Loess Plateau. (a) Daily time series of pore water table depth (blue line) and surface
 748 temperature (red line) from September 2023 to November 2024. The water table fluctuates seasonally,
 749 rising from \sim -8.1 m in late summer to a maximum of \sim -5.0 m in early spring (March 2024), indicating
 750 delayed infiltration and cool-season recharge. (b) Daily precipitation (blue bars) and modeled pore water
 751 recharge estimates using the RISE and MRC methods. (c) Daily precipitation (blue bars) and modeled
 752 pore water recharge estimates using the RISE methods. Most recharge events occur from October to
 753 April, even when rainfall is not especially high, while warm-season precipitation contributes little to
 754 recharge—likely due to increased evaporative losses and shallow soil retention. Together, these patterns
 755 suggest strong seasonal control on recharge processes, with effective infiltration primarily occurring
 756 during cooler, low-evaporation periods.

757

758 **5.6. Discussion**

759 **6.5.1. Isotopic compositions of various water bodies in the gully region**

760 In hydrological studies, the isotopic composition of water bodies reflects both sources and changes
761 in hydrological processes (Wan and Liu, 2016; Kumar et al., 2019; Dasgupta et al., 2024). Precipitation,
762 surface water, and groundwater usually exhibit differences in isotopic characteristics due to variations in
763 evaporation, infiltration, and mixing (Gleeson et al., 2016; Kuang et al., 2019; Al-Oqaili et al., 2020).
764 However, similar isotopic distributions among different water bodies often indicate a strong hydrological
765 connection in their water sources (Yang and Wang, 2023).

766 Our study found that rainfall and pond water have similar spatial isotopic distribution patterns,
767 indicating that pond water primarily originates from rainfall. This reflects the region's geographical and
768 hydrological characteristics. In this severely eroded gully region, the local government has constructed
769 an extensive network of ponds and check dams to capture hillside runoff (Liu et al., 2017; Xue et al.,
770 2025). As a result, most precipitation from the hills converges into these gully ponds and check dams. A
771 lower pond water line slope indicates evaporation fractionation during retention. Evaporation
772 preferentially removes lighter isotopes (^1H and ^{16}O), enriching heavier isotopes (^2H and ^{18}O) and shifting
773 the pond water's isotopic composition from its precipitation source (Aragu et al., 1998; Zhang and Wu,
774 2009; Gleeson et al., 2016). This similarity is primarily due to the fact that pond water originates from
775 rainfall and its runoff in the hilly-gully region (Liu et al., 2011; Ji et al., 2024). Additionally, the isotopic
776 values of most groundwater in the gully areas are more depleted compared to those of rainfall and pond
777 water, likely due to the recharge mechanisms and residence times of different groundwater types, and the
778 inherent isotopic characteristics of their primary recharge sources (Ouali et al., 2024). The depleted
779 signatures in groundwater reflect preferential capture of isotopically light summer monsoon events, with
780 effective percolation delayed to cooler seasons due to transient soil storage and minimized evaporation
781 —, consistent with observed water table rises predominantly from October to April. Nevertheless, these
782 values fall within the range of precipitation isotopic values, leaning towards the more negative end. This
783 suggests two complementary mechanisms: (1) the thin unsaturated zone (<10 meters) provides
784 preferential pathways for rapid infiltration of precipitation, minimizing evaporative fractionation, and (2)
785 groundwater is likely recharged primarily by intense precipitation events (e.g., summer storms) with
786 inherently more negative isotopic signatures (Liu, 2024). Together, these processes explain the observed
787 isotopic characteristics of groundwater. Additionally, the isotopic values of most groundwater in the gully

788 ~~areas are more depleted compared to those of rainfall and pond water, likely due to the recharge~~
789 ~~mechanisms and residence times of the different groundwater types (Ouali et al., 2024). Nevertheless,~~
790 ~~these values fall within the range of precipitation isotopic values, leaning towards the more negative end,~~
791 ~~suggesting that groundwater is likely directly recharged by significant precipitation events. This is due~~
792 ~~to the thin unsaturated zone (<10 m) in the gully areas, which facilitates rapid infiltration and direct~~
793 ~~recharge from heavy rainfall.~~

794 To further investigate the complexity of different types of groundwater in the gully area, we
795 conducted hydrological and geological surveys, collecting water samples from spring water, pore water,
796 and fissure water. The results show that the isotopic values of spring water, pore water, and fissure water
797 are closely clustered, indicating a strong interconnection among the different types of groundwater within
798 the hydrological cycle. This is likely due to their shared geological and hydrological environments
799 (Bouwer, 2002; Li et al., 2021; Zhang et al., 2022). Our study found that the water line slope of pore
800 water and fissure water was higher in the dry season than in the rainy season, with values falling between
801 the slopes of pond water from the rainy and dry seasons. To investigate the cause of these results, we
802 analyzed groundwater level dynamics, which showed that water tables were lower at the end of the rainy
803 season but rebounded afterward, making dry-season tables higher. This suggests that rainy-season
804 groundwater mixes with evaporatively enriched water, lowering its slope, while dry-season groundwater
805 is recharged by delayed rainfall and pond water, increasing its slope. These findings reveal that isotopic
806 composition is influenced by both current and prior hydrological conditions. They also highlight the
807 complexity of evaporation fractionation regulated by water mixing and demonstrate the significant
808 impact of pond construction on groundwater recharge and regional hydrology in the gully regions.

809

810 **6.2. Groundwater recharge processes in the gully region**

811 In recent years, discussions of groundwater recharge sources on the Loess Plateau have largely
812 focused on tableland and hilly areas characterized by thick loess deposits, whereas gully regions have
813 received comparatively limited attention (Li et al., 2017; Xiang, 2020; Lu, 2020). For instance, Liu et al.
814 (2011) demonstrated that groundwater near valley bottoms in hilly loess areas can be replenished by a
815 combination of precipitation, runoff, and surface water. Our results are broadly consistent with these
816 earlier findings, but extend them by providing multiple lines of site-specific evidence. Based on stable
817 isotope signatures and chloride concentrations, we independently identify precipitation and surface water

818 as the primary sources of groundwater recharge in gully systems. Furthermore, by applying a structural
819 equation model (SEM), we quantitatively evaluate the relative importance of different recharge pathways,
820 demonstrating that surface water (particularly pond water) plays a key mediating role in transferring
821 precipitation inputs to subsurface pore water. Building on these results, we classify groundwater in the
822 study area into three functional types, spring water, pore water, and fissure water, and propose a
823 progressive, multi-stage recharge framework: (1) direct recharge of pond water by precipitation and
824 indirect recharge of pore water by precipitation; (2) focused recharge from pond water to pore water; and
825 (3) downward percolation from pore water to fissure water. This framework highlights the complexity of
826 groundwater flow and recharge processes in gully-dominated landscapes and underscores the significant
827 influence of human interventions, such as ponds and check dams, on modifying hydrological
828 connectivity and recharge dynamics.~~In recent years, discussions of groundwater recharge sources have~~
829 ~~primarily focused on tableland and hilly areas with thick loess deposits, although only a few researchers~~
830 ~~have examined gully regions (Li et al., 2017; Xiang, 2020; Lu, 2020). For example, Liu et al. (2011)~~
831 ~~found that groundwater near valleys in the hilly loess area is replenished by precipitation, runoff, and~~
832 ~~surface water. Our findings support this study, identifying rainfall and surface water as major sources of~~
833 ~~gully groundwater recharge. We classify groundwater into three types (spring water, pore water, and~~
834 ~~fissure water) and propose a gradual recharge process, including (1) direct and indirect recharge from~~
835 ~~precipitation to pond water and pore water, respectively; (2) concentrated recharge from pond water to~~
836 ~~pore water; and (3) percolation recharge from pore water to fissure water. This reflects the complexity of~~
837 ~~the groundwater system and the significant impact of human activities (e.g., ponds and check dams) on~~
838 ~~hydrological processes.~~

839 In the deep-profile unsaturated zones of the hilly region on the Loess Plateau, previous studies have
840 used chloride mass balance and tritium peak methods to estimate groundwater recharge from
841 precipitation, typically accounting for 2%–22% of annual rainfall, with water residence times in the
842 unsaturated zone lasting several years or even hundreds of years (Huang ~~et al.~~ and Pang, 2011; Tan et al.,
843 2016; Li et al., 2017; Wang et al., 2024). However, these studies did not address the catchment role of
844 gully regions. Field observations and past studies show that precipitation rarely directly infiltrates thick
845 loess in hilly areas (Xu et al., 1993; Li, 2001). Instead, it forms surface runoff that converges into
846 engineered gullies and accumulates in ponds or other water bodies (perched water), serving as a
847 concentrated recharge source for groundwater (Yu et al., 2025), reflecting the sustained and delayed

848 impact of gully runoff on groundwater recharge, which is consistent with the results of this study. In
849 summary, while hillslope-scale studies describe a “dispersed recharge” mode, where precipitation
850 percolates slowly through thick unsaturated zones, this study identifies a “concentrated recharge” mode
851 in engineered gullies, driven by runoff convergence and regulated by check dams via ponding. These
852 fundamentally distinct modes, differing in hydrological processes, spatial scales, and recharge
853 efficiencies, collectively enhance the understanding of groundwater recharge mechanisms on the Loess
854 Plateau.

855 Notably, our study does not consider confined water. Tan et al. (2016) indicated that the groundwater
856 in the high mountain-hilly loess aquifer does not originate from the upwelling of ancient regional
857 groundwater, and there is no evidence of deep confined water beneath the loess strata in the high
858 mountain-hills. Additionally, our findings represent only the groundwater recharge results in the gully
859 regions for two reasons: (1) The hydrological system is complex, with significant variations across
860 different landscapes of the Loess Plateau (Li et al., 2019; Li et al., 2021). For example, Li et al. (2019)
861 found that groundwater dominates the hydrological system in the tableland on the Loess Plateau, where
862 surface water (streams) is recharged by groundwater because river channels are deeper than the bedrock.
863 (2) Our data collection focused on gully because the “Loess Liang” and “Loess Mao” hillside areas are
864 covered by thick loess with minimal water sources.

865

866 **6.3. Groundwater recharge rates in the gully region**

867 In many parts of the world, identifying the sources of groundwater recharge and its renewability is
868 essential for effective water resource management (Ajur and Baalousha, 2021; Meles et al., 2024). In
869 the hilly-gully region of the Loess Plateau, where groundwater is considered a crucial source of safe
870 water, understanding the origins and recharge of aquifers provides valuable information for water
871 resource planners (Wang et al., 2006; Liu et al., 2011; Wang et al., 2024). This knowledge is essential
872 and should be shared with regions facing similar challenges.

873 Groundwater recharge can be quantified from three hydrological sources: surface water, the
874 unsaturated zone, and the saturated zone (Scanlon et al., 2022). Recharge estimates based on the saturated
875 zone are generally more reliable than those from the unsaturated zone, as the latter represents potential
876 recharge that may not ultimately reach the groundwater table (Beven and Germann, 2013; Huang ~~et~~
877 ~~al.~~ and Shao, 2019). The groundwater table fluctuation method is widely used for estimating saturated

878 zone recharge due to its high temporal resolution and intuitive nature (Gumuła-Kawęcka et al., 2022; Xu
879 et al., 2024). In our study area, ITTPs estimated similar transit times for both pore water and fissure water.
880 Therefore, we used the groundwater table fluctuation method to assess the recharge of pore water in the
881 gully region. The total recharge from 2023 to 2024 was estimated at 241.4 ± 6.0 mm and 238 ± 6.0 mm
882 using the MRC and RISE methods, respectively. Under constant specific yield conditions, the MRC
883 method typically estimates higher groundwater recharge and recharge days than RISE, as it accounts for
884 groundwater table decline due to lateral outflow and other discharge processes in the absence of recharge
885 (Heppner and Nimmo, 2005). Our findings support this pattern. Furthermore, the key parameter for
886 estimating groundwater recharge using the water table fluctuation method is specific yield (S_y), which
887 depends on soil properties and water table depth (Liang et al., 2016). Shallow soil measurements (0–50
888 cm) using the test pit method (total porosity minus field capacity) yielded $S_y \approx 0.03$, consistent with high
889 capillary retention in near-surface loess (Wang et al., 2024). However, for water tables deeper than 2 m
890 (as in this study, typically 4–10 m), the test pit method provides a reliable estimate of aquifer-scale
891 drainable porosity (Nachabe, 2002; Shah and Ross, 2009; Liang et al., 2016). Accordingly, we adopted
892 $S_y = 0.032$, aligned with values of ~ 0.03 reported for similar loess-derived unconfined aquifers on the
893 Loess Plateau (Wang et al., 2023). Sensitivity analysis indicates that recharge estimates vary by
894 approximately $\pm 25\%$ across the plausible S_y range (0.032 ± 0.008), reflecting uncertainty in effective
895 drainable porosity within shallow gully aquifers. Uncertainty analysis showed that recharge estimates
896 vary by $\pm 25\%$ for S_y , which ranges from $3.2 \pm 0.8\%$.

897 ~~the key parameter for estimating groundwater recharge using the groundwater table fluctuation~~
898 ~~method is specific yield, which depends on factors such as soil properties and water table depth. This~~
899 ~~value can be derived from empirical soil texture, pumping tests, or the test pit method (Nachabe, 2002;~~
900 ~~Liang et al., 2016). Shah and Ross (2009) found the test pit method reliable for water tables deeper than~~
901 ~~2 m. In this study, with a water table exceeding 2 m, the specific yield was 0.32, consistent with values~~
902 ~~of 0.3 in similar soil conditions (Wang et al., 2023).~~

903 Research on groundwater recharge in the Loess Plateau has mainly focused on deep-profile
904 unsaturated zones in the tableland and hilly areas, with tracer methods estimating recharge between 9 to
905 100 mm (Huang et al. and Pang, 2011; Li et al., 2017; Xiang et al., 2019; Lu, 2020; Wang et al., 2024).
906 In contrast, our study in the gully region indicates recharge of up to 240 mm, much higher than previous
907 estimates on deep-profile unsaturated zones. This difference reflects several factors: 1) Unsaturated zone

908 thickness—; In the gully region, the unsaturated zone is generally less than 10 m thick, much shallower
909 than in tableland and hilly areas (mean thickness of 92.2 m), making infiltration easier and promoting
910 effective recharge. 2) Gully topography and hydrology—, characterized by well-developed channels,
911 concentrated runoff, and widespread ponds and check dams—, promote focused infiltration (Liu et al.,
912 2017; Li et al., 2021; Xue et al., 2025). 3) Research methods—; Tracer methods reflect long-term
913 recharge rates and are better suited for thicker unsaturated zones (Huang ~~et al.~~ and Pang, 2011; Lu, 2020;
914 Li et al., 2017). In contrast, the water table fluctuation method directly captures short-term recharge
915 dynamics and works better in thinner unsaturated zones. Moreover, this method also better captures
916 surface water-groundwater interactions and focused recharge effects (Gumuła-Kawęcka et al., 2022).
917 These findings underscore the importance of studying recharge in gully regions, filling a research gap in
918 the Loess Plateau's geomorphology and providing new ecohydrological insights. However, the
919 robustness of our findings requires further exploration. On one hand, due to the limited spatial
920 distribution of sampling points, the current results primarily reflect the hydrological characteristics of
921 engineered/localized typical gullies, and their representativeness at the regional scale requires validation
922 through future expansion of the monitoring network. On the other hand, the study period did not
923 encompass extreme precipitation or drought events, which may significantly alter surface flow
924 convergence conditions and vadose zone water transport mechanisms, thereby substantially impacting
925 recharge processes. Future work should strengthen dynamic monitoring and simulation analysis under
926 extreme hydrological scenarios. ~~Furthermore, our study demonstrates the potential of artificial ponds to~~
927 ~~regulate water resources and enhance recharge, with valuable implications for water management and~~
928 ~~ecological engineering.~~

929

930 **6.4. Revised conceptual model**

931 To convey our evolving understanding of the spatial structure and dynamics in the Gully Region,
932 we developed a conceptual model that traces precipitation's transformation into subsurface water, from
933 runoff capture and surface ponding in dammed gullies/gully reaches, through infiltration in the
934 unsaturated zone, to recharge in both the shallow— porous aquifer and deeper bedrock fissure systems
935 (Figure 11). ~~Through this integrative framework, we elucidate the transformation of precipitation into~~
936 ~~various forms of subsurface water by explicitly tracing its movement through a cascade of~~
937 ~~compartments— from surface ponding in dammed gullies, to infiltration through the unsaturated zone,~~

938 ~~and eventual recharge into both the porous aquifer and underlying bedrock fissure systems.~~ This
939 conceptual reframing is grounded in the stark contrasts between hydrological processes active on hilly
940 uplands and managed gully systems. In the hilly uplands, previous studies have shown that thick loess
941 deposits—, often exceeding 90 m (including low-permeability aquifers)—, combined with steep slopes
942 (>15°) severely restrict vertical infiltration (Zhu et al., 2018; Huang et al., 2019; Huang et al., 2024).
943 Compounded by short-duration, high-intensity rainfall events that provide insufficient moisture for deep
944 profile wetting, rainfall is converted rapidly into surface runoff (Li et al., 2021; ~~Zhu et al., 2018~~). Our
945 new work shows that ~~This~~ runoff is systematically funneled downslope into gully systems, ~~a process~~
946 further intensified as a consequence of ecological engineered check dams and retention ponds that
947 intercept and concentrate overland flow. ~~Because precipitation seldom infiltrates directly into the thick~~
948 ~~loess of upland regions (Xu et al., 1993; Li, 2001), m.~~ Most infiltration occurs after surface water
949 accumulates in fill zones of engineered gullies—. Ponds and perched water bodies subsequently serve as
950 focal points for groundwater recharge localized recharge foci. (~~Yu et al., 2025~~).

951 Crucially, gully systems possess distinct hydrogeological characteristics: the loess mantle is much
952 thinner (typically < 25 m), and the soils are dominated by silt loam textures with moderate specific yield
953 (0.02–0.05) and high field capacity (21–28%). These properties promote transient water storage and
954 enable temporally delayed and, depth-partitioned infiltration. Based on our integrated analyses of stable
955 isotopes, chloride concentrations, and inverse transit time proxies, we find that engineered gullies
956 function not as passive erosional features but as active, managed recharge conduits. ~~gullies function not~~
957 ~~as passive erosional features but as active recharge conduits.~~ This conceptualization captures a critical
958 spatial transition—, from runoff generation in the hilly uplands to focused recharge in gully zones—,
959 emphasizing the pivotal role of gully systems in regulating groundwater recharge across the Loess
960 Plateau landscape.

961 Combined hydrological monitoring and multi-indicator analysis further reveal that following the
962 rainy season, infiltration depths on hilly slopes are typically shallow— (less than 1 m), —while
963 groundwater levels in gully areas exhibit pronounced rises exceeding 2 m (Fig. 11). Recharge estimates
964 based on the water table fluctuations reach up to approximately 240 mm at the monitored gully reach,
965 far surpassing values observed in deep unsaturated zones of tablelands and hills (Huang ~~et al.~~ and Pang,
966 2011; Li et al., 2017; Lu, 2020; Wang et al., 2024). The results of this study reinforce the role of
967 engineered –gulliesy reaches –as focal points for groundwater recharge and further quantify site-scale

968 [pore-water recharge equivalent to ~43% of mean annual precipitation, a finding that highlights the](#)
969 [efficiency of focused infiltration under managed conditions.~~the recharge rate of pore water at 43%, a~~
970 \[crucial finding for understanding groundwater recharge mechanisms in semi-arid regions.~~These results~~
971 ~~reinforce the role of gullies as focal points for groundwater recharge and are consistent with prior studies.~~
972 ~~For instance, in hilly areas, precipitation rarely recharges groundwater due to the thick loess layers, with~~
973 ~~an average infiltration depth of only 1 meter \\(Wang et al., 2024\\).~~ This value reflects spatially focused
974 recharge under conditions of runoff convergence and ponding, and should not be interpreted as
975 representative of hillslope or catchment-wide recharge rates.\]\(#\)](#)

976 Liu et al. (2011) found that groundwater near valleys in the hilly loess area is replenished by
977 precipitation, runoff, and surface water. Moreover, fissure water exhibits more depleted isotopic
978 signatures and higher chloride concentrations, indicating deeper percolation of pore water or mixing with
979 older recharge sources (Fig. 11). These patterns, supported by ITTPs and [statistical \(SEM-based\)](#)
980 [connectivity indicators](#)~~partial SEM linkages~~, reveal a hierarchical recharge sequence: event-driven
981 infiltration enters [the shallow-pore porous shallow](#) aquifer, some of which slowly percolates into deeper
982 fissure zones. This hierarchical mechanism is facilitated by the combination of thin loess mantles,
983 engineered interventions (e.g., check dams and ponds), and delayed hydrological responses.

984 By integrating multiple lines of evidence, this conceptual model redefines [engineered](#) gullies as
985 selective recharge corridors [whose hydrological function emerges from the interaction between](#)~~shaped~~
986 ~~by both~~ geomorphic structure and human intervention. It challenges the traditional view of gullies as
987 purely erosional landforms and emphasizes their dual hydrological function: acting both as runoff
988 conveyance channels and as transient reservoirs that store and redistribute water across space and time.
989 This recharge capacity is jointly governed by topographic convergence, reduced loess thickness, and the
990 presence of engineered structures such as check dams and retention ponds: [that increase residence time.](#)

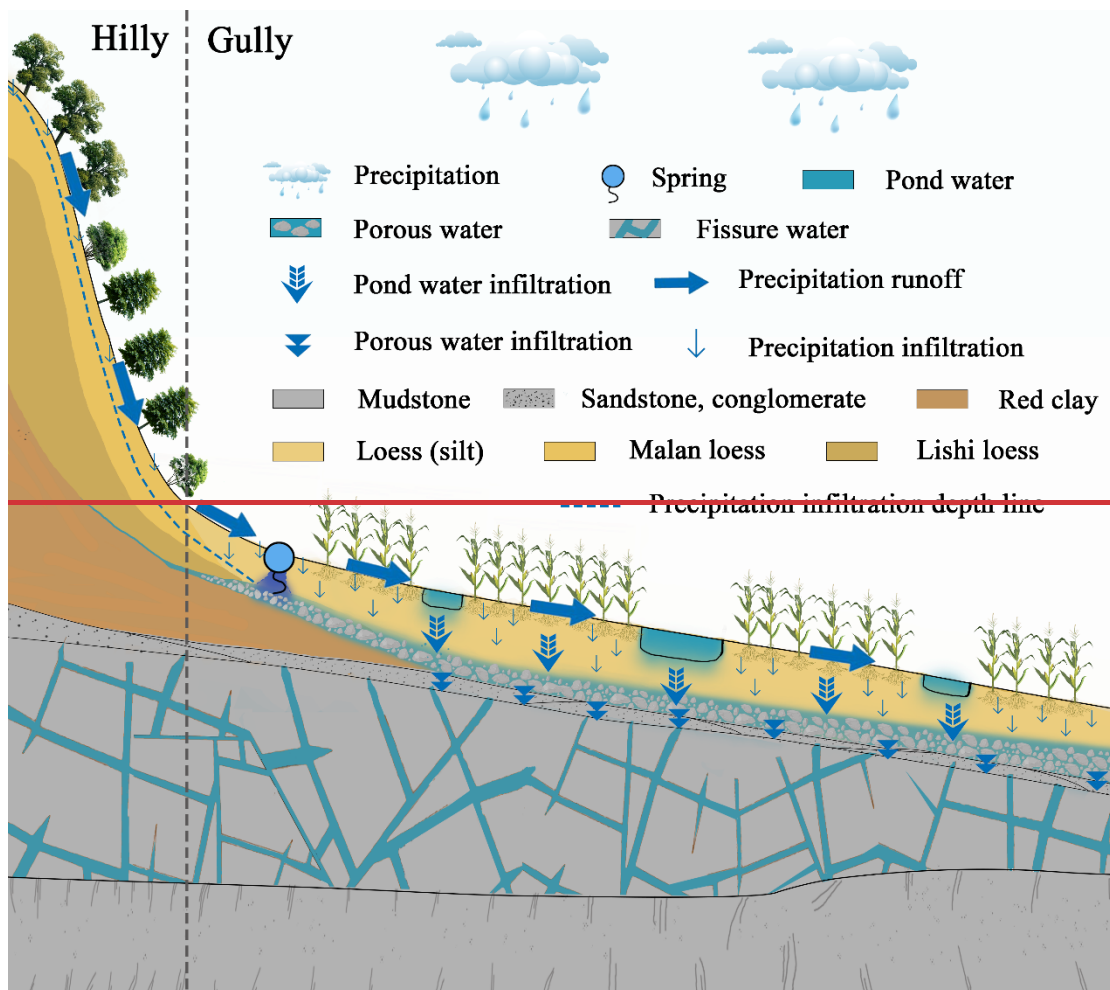
991 Crucially, the model offers insight into the multifunctionality of ecological engineering—
992 particularly check dams and ponds—[in enhancing groundwater recharge, and supporting ecosystem](#)
993 [restoration hydrological regulation, water security, and ecosystem restoration](#) across the Loess Plateau.
994 [This study proposes a cascade-type recharge framework for engineered gully systems, highlighting the](#)
995 [role of engineered gullies as convergence pathways that locally focus infiltration and groundwater](#)
996 [recharge. Rather than invoking preferential flow within the soil matrix, this framework emphasizes](#)
997 [topographic convergence, stratigraphic thinning, and engineered ponding as the dominant mechanisms](#)

1098 [that promote spatially concentrated recharge within gully zones. While this process is demonstrated using](#)
1099 [site-specific tracer and water-table observations, its broader relevance at the catchment scale remains](#)
1100 [conceptual and warrants further investigation. This study identifies a distinctive cascade type recharge](#)
1101 [process in loess gully catchments and proposes the “gully dominated preferential recharge mechanism”.](#)
1102 [This mechanism emphasizes the hydrological function of gullies as convergence pathways and efficient](#)
1103 [recharge windows at the catchment scale, rather than preferential flow paths within the soil matrix.](#)
1104 [Furthermore, water movement within the silted loess layer of the gully system remains dominated by a](#)
1105 [piston flow pattern \(Yu et al., 2025\). Compared to the traditional piston flow and preferential flow models](#)
1106 [commonly applied in the region, the proposed “gully dominated preferential recharge mechanism” marks](#)
1107 [a notable theoretical advancement. Whereas previous models primarily emphasize vertical infiltration](#)
1108 [through homogeneous loess layers, this study is the first to quantitatively identify a cascade recharge](#)
1109 [process unique to thin loess gully catchments.](#) By identifying the pivotal role of gully systems in
1110 stormwater detention, delayed infiltration, and [multi aquifer depth-partitioned](#) recharge, this study
1111 establishes a [robust theoretical and technical foundation for mechanistically grounded conceptual basis](#)
1112 improving water resource allocation, infrastructure planning, and groundwater sustainability in arid and
1113 semi-arid regions.

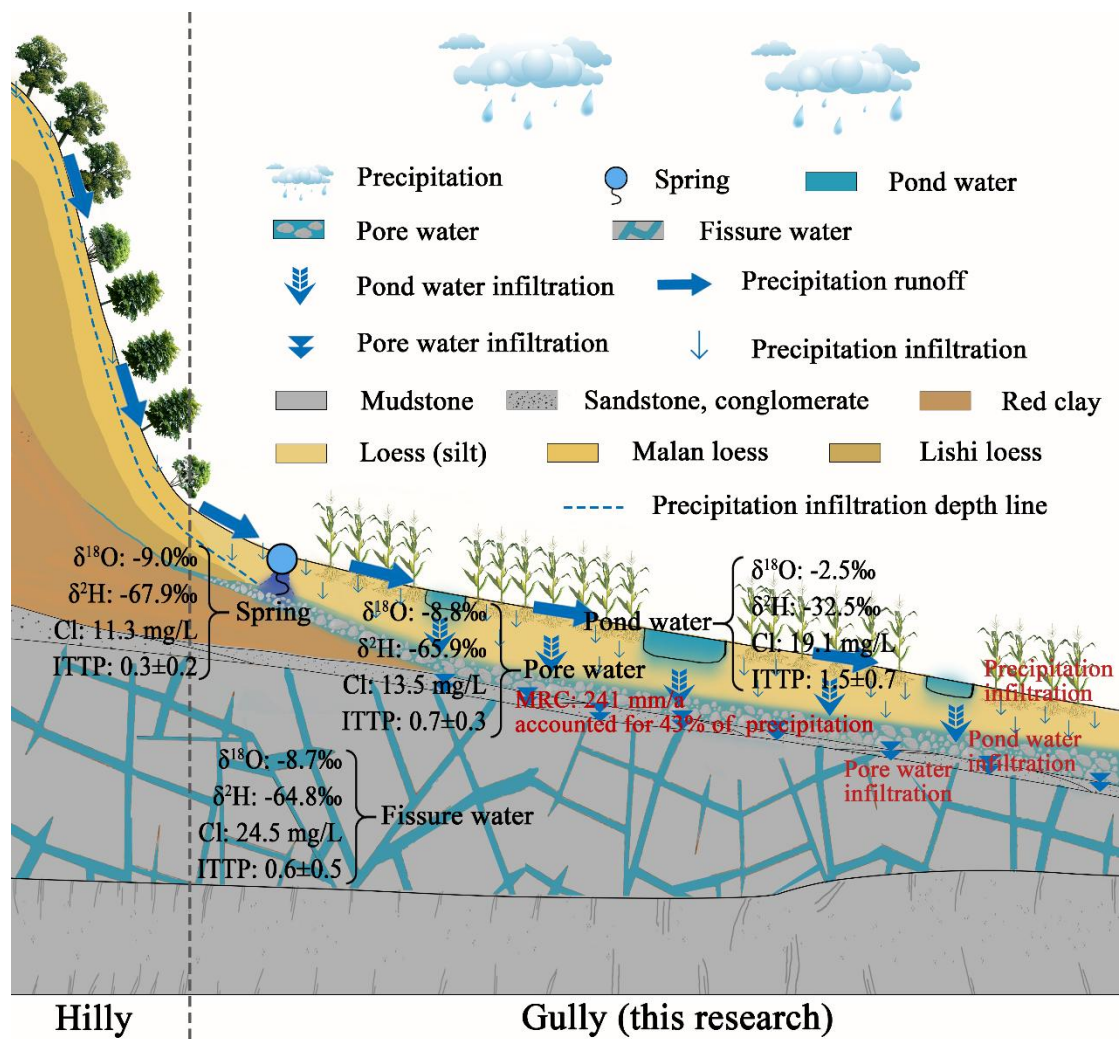
1114 [However, with the reconstruction of gully systems and ecological restoration, attention must also](#)
1115 [be given to the potential risks of pollutant migration \(Yu et al., 2020\). The hydrological functions of](#)
1116 [gullies may enhance the movement of pollutants into groundwater, especially in areas with intensive](#)
1117 [human activities, where pollutants can enter engineered gullies through surface runoff and subsequently](#)
1118 [infiltrate the groundwater system. During ecological restoration, excessive human intervention or soil](#)
1119 [improvement measures may lead to the accumulation and dispersion of pollutants, which may](#)
1120 [compromise groundwater security \(Liu et al., 2017\). Therefore, the protection and rational reconstruction](#)
1121 [of gully systems should not only focus on their hydrological functions but also consider potential](#)
1122 [environmental risks, particularly the pathways of pollutant migration. These findings therefore](#)
1123 [underscore the need to evaluate gully-based restoration strategies within an integrated water-quality and](#)
1124 [groundwater-protection framework \(Obuobie et al., 2012; Zhao et al., 2019; Zhao and Wang, 2021; Xue](#)
1125 [et al., 2025\). More importantly, these findings have direct implications for land management practices](#)
1126 [and ecological restoration strategies in similar arid regions worldwide.](#)

1127 [The study demonstrates how hydrologically arrested gully systems can function gullies serve as](#)

1028 critical “recharge windows” for groundwater in arid areas. This underscores the importance of
 1029 systematicallystrategically identifying and ~~conserving~~managing natural–gully networks in watershed
 1030 management, while avoiding excessive filling or hardening to preserve their hydrological functions. In
 1031 ecological restoration projects, directing surface runoff toward engineered gullies under controlled
 1032 conditions can efficiently convert limited precipitation into groundwater storage, thereby enhancing
 1033 regional water retention capacity. Beyond advancing theoretical understanding of regional hydrological
 1034 processes, ~~it also~~ this conceptual model provides ~~a sound basis~~ a process-based foundation for developing
 1035 spatially targeted models of groundwater recharge in managed dryland landscapes.-



1036



1037

1038

1039

1040

1041

1042

1043

1044

1045

1046

1047

1048

1049

1050

Fig. 4011. Hydraulic connections between different water bodies in the hilly-gully region of the Loess Plateau. The study area consists of hilly and gully regions. In the hilly area, the stratigraphic sequence from top to bottom is Malan loess, Lishi loess, red clay, sandstone, and mudstone. Rainfall infiltration within the Malan loess is less than 1 m, and the area is mainly covered by vegetation. In the gully area, the stratigraphy from top to bottom includes loess (silt), sandstone and conglomerate, and mudstone. Pore water is found within the sandstone and conglomerate, while fissure water occurs in bedrock fractures (mudstone). Numerous check dams or ponds are distributed throughout the gully area. The vertical separation between the pore water and pond water ranges from 3 to 5 m. Corn is the main crop cultivated in this region. Most springs in the study area are located at the junction of the hilly and gully regions and are discharged from pore water.

65.5. Limitations and future research directions

This study underscores the limitations of relying on a single indicator to infer [localized](#) groundwater

1051 recharge pathways, as doing so may lead to oversimplified or potentially misleading interpretations of
1052 complex hydrological processes. While stable isotope signatures suggest precipitation contributes to pore
1053 aquifer recharge, they do not provide clear evidence of direct recharge from pond water to either pore or
1054 fissure groundwater during the dry season. In contrast, the spatial distribution of chloride concentrations
1055 offers compelling support for focused pond water leakage into the shallow groundwater system.

1056 Without explicit mass-balance constraints, structural equation modeling may not independently or
1057 quantitatively represent actual groundwater flow processes. In contrast, the water-table fluctuation
1058 method, which directly measures changes in groundwater levels, provides a more empirically grounded
1059 estimate of total recharge. Each approach nevertheless offers distinct strengths: water-table fluctuations
1060 resolve the timing and magnitude of recharge, whereas isotopic, hydrochemical, and modeling analyses
1061 yield critical insights into recharge sources and flow pathways. By leveraging the complementarity and
1062 mutual corroboration of these methods, our study robustly demonstrates the pivotal role of gully areas in
1063 regional groundwater recharge. Although variance decomposition analysis and structural equation
1064 modeling suggest statistical linkages among different water bodies and provide useful clues about
1065 potential recharge pathways, these associations may be confounded by overlapping isotopic signatures
1066 or by non-conservative processes such as evaporation and mixing, potentially leading to an
1067 overestimation of hydrological connectivity. In the absence of mass balance constraints, the pathways
1068 inferred through SEM may not accurately reflect the actual flow processes within the groundwater system.
1069 By contrast, the water table fluctuation method captures both vertical and lateral recharge processes,
1070 yielding estimates that are more likely to reflect actual recharge rates. Drawing on this empirical evidence,
1071 the present study further substantiates the critical role of gully zones in regional groundwater recharge.

1072 Despite effort to address uncertainties, limitations remain in terms of spatial and temporal sampling
1073 density. For example, the lack of long-term tracers such as groundwater age, combined with limited
1074 observations of groundwater level fluctuations, constrains our ability to assess recharge dynamics over
1075 multi-year timescales. Additionally, the current sampling design includes only two campaigns during the
1076 rainy and dry seasons, which may be insufficient to fully capture the seasonal variability of ITTP values.
1077 This, in turn, may affect the accuracy of groundwater renewal frequency estimates and the strength of
1078 inferred hydrological connections. In arid and semi-arid regions, groundwater recharge is typically
1079 triggered by infrequent, high-intensity rainfall events. However, existing sampling strategies based on
1080 seasonal intervals often lack the temporal resolution necessary to capture these short-lived, event-driven

1081 recharge processes effectively.

1082 Future research should address these issues through several improvements: (1) conducting higher-
1083 frequency, event-scale sampling to systematically monitor rainfall, spring discharge, and pond water
1084 level dynamics, thus capturing the influence of key hydrological events on recharge processes; (2)
1085 expanding the spatial coverage of pore and fissure well monitoring to improve the accuracy of regional
1086 recharge pattern identification; and (3) incorporating additional environmental tracers (e.g., ^3H , ^{22}Na) to
1087 trace flow paths and estimate recharge lag times. In addition, systematic observation of event-scale
1088 hydrological processes should be strengthened by establishing a high-frequency, event-driven monitoring
1089 network to better capture the nonlinear coupling among rainfall, surface runoff, and groundwater
1090 dynamics. This approach would significantly improve our understanding of rapid infiltration events and
1091 associated recharge mechanisms.

1092 From a methodological perspective, integrating statistical techniques—, such as SEM and variance
1093 decomposition analysis—, with process-based physical models like MODFLOW and HYDRUS can
1094 provide mechanistically constrained insights into recharge pathways. Compared to correlation-based
1095 statistical methods, physical models offer greater precision in characterizing groundwater flow and
1096 recharge processes across both temporal and spatial dimensions, helping to reduce uncertainties
1097 associated with non-conservative tracer behavior and the absence of mass balance constraints. Regarding
1098 measurements, hydrometric instrumentation within check dams and beneath pond beds could further
1099 quantify the recharge effects of various engineering interventions under specific hydrological conditions.
1100 Additionally, integrating isotopic data with mean transit time modeling, combined with targeted
1101 [catchment-wide](#) field monitoring and improved spatial analysis, could help elucidate recharge pathways,
1102 quantify temporal dynamics, and enhance process-level understanding of groundwater recharge [in](#)
1103 [throughout the catchment of suche](#) complex dryland landscapes. Collectively, these efforts will contribute
1104 to a stronger theoretical foundation and offer practical guidance for the precise management of water
1105 resources, the design of ecologically appropriate engineering interventions, and the implementation of
1106 effective landscape rehabilitation strategies.

1107

1108 **76. Conclusion**

1109 [Through integrated analysis of stable isotopes, chloride concentrations, water-table fluctuations, and](#)

1110 inverse transit time proxies, this study provides multiple, convergent lines of evidence that engineered
1111 gully reaches on the Loess Plateau function as hydrologically significant recharge zones, rather than
1112 solely as products of accelerated erosion and degradation. Precipitation-driven runoff supports
1113 substantial recharge to shallow pore aquifers, with site-scale recharge magnitudes equivalent to
1114 approximately 43% of mean annual precipitation at the monitored gully reach. Although evaporative
1115 fractionation limits the ability of stable isotopes alone to resolve direct recharge from ponded surface
1116 water, chloride concentrations provide independent evidence consistent with mixing between pond water
1117 and pore water, complementing the isotopic patterns. Together, these indicators indicate likely hydraulic
1118 connectivity, while not constituting a mass-balanced quantification of recharge sources. Recharge within
1119 shallow gully-zone aquifers is spatially concentrated and temporally selective, governed by topographic
1120 convergence, loess stratigraphy, and ecological engineering structures—, particularly check dams and
1121 ponds—that, which increase surface-water residence time and promote focused infiltration. Through
1122 integrated analysis of stable isotopes, chloride concentrations, water table fluctuations, and inverse transit
1123 time proxies, we developed multiple lines of evidence to reframe gullies in the Loess Plateau as
1124 hydrologically significant recharge zones, rather than solely as indicators of erosion and degradation.
1125 Precipitation events drive substantial recharge to shallow pore aquifers, with annual rates exceeding
1126 238 mm⁴³, accounting for a large fraction of annual rainfall. While isotopic evidence for recharge
1127 from pond water is obscured by evaporative fractionation, chloride concentrations, stable isotopes, and
1128 SEM provide a clear signal of subsurface connectivity. Recharge in this system is both spatially
1129 concentrated and temporally selective, shaped by terrain configuration, loess stratigraphy, and ecological
1130 engineering structures such as check dams and ponds.

1131 These findings offer a process-based foundation framework for developing hydrological indicators
1132 of landscape function and restoration performance managed in dryland environments. Specifically,
1133 recharge magnitude, isotopic damping, and solute accumulation patterns may serve as diagnostic tools
1134 indicators for identifying effective recharge zones and tracking system responses hydrological response
1135 to intervention. To refine these indicators, future studies should incorporate high-frequency monitoring,
1136 event-based sampling, and multi-tracer approaches. Collectively, this work challenges conventional
1137 views of gullies as hydrological liabilities and demonstrates context-dependent role as targeted recharge
1138 assets in engineered dryland systems, refining conceptual understanding of dryland groundwater
1139 recharge and informing the evaluation and design of ecological engineering strategies in similar semi-

1140 ~~arid landscapes, their underappreciated role as targeted recharge assets , advancing dryland~~
1141 ~~groundwater sustainability and providing actionable insights for landscape-scale ecological restoration~~
1142 ~~and management.~~

1143

1144

1145

1146 **Author contributions:**

1147 ZXJ: Conceptualization, Methodology, Formal analysis, Investigation, Visualization, Data curation,
1148 Validation, Writing-original draft. ADZ: Conceptualization, Formal analysis, Validation, Visualization,
1149 Writing-review & editing. LW: Conceptualization, Funding acquisition, Project administration,
1150 Resources, Supervision, Visualization, Writing-review & editing.

1151 **Data availability:**

1152 ~~All datasets are available at Zenodo: <https://zenodo.org/records/18596600>. Data are available from the~~
1153 ~~corresponding author upon reasonable request.~~

1154 **Conflicts of Interest:**

1155 The contact author has declared that none of the authors has any competing interests.

1156 **Acknowledgments:**

1157 This work was supported by the National Natural Science Foundation of China (grant numbers 42377318
1158 and U24A20629).

1159

1160 **References**

- 1161 Ajjur, S.B., Baalousha, H.M. A review on implementing managed aquifer recharge in the Middle East
1162 and North Africa region: methods, progress and challenges. *Water International*. 46(4): 578-604, 2021.
1163 <https://doi.org/DOI: 10.1080/02508060.2021.1889192>.
- 1164 Al-Oqaili, F., Good, S.P., Peters, R.T., Finkenbiner, C., Sarwar, A. Using stable water isotopes to assess
1165 the influence of irrigation structural configurations on evaporation losses in semiarid agricultural systems.
1166 *Agricultural and Forest Meteorology*. 291: 108083, 2020. [https://doi.org/DOI:](https://doi.org/DOI: 10.1016/j.agrformet.2020.108083)
1167 [10.1016/j.agrformet.2020.108083](https://doi.org/DOI: 10.1016/j.agrformet.2020.108083).
- 1168 Aragu, L., Froehlich, K., Rozanski, K. Stable isotope composition of precipitation over southeast Asia.
1169 *Journal of Geophysical Research*. 103(28): 721-728, 1998. <https://doi.org/DOI: 10.1029/98JD02582>.
- 1170 Berg, A., Findell, K., Lintner, B., Giannini, A., Seneviratne, S.I., Hurk, B.V.D., Lorenz, R., Pitman, A.,
1171 Hagemann, S., Meier, A. Land-atmosphere feedbacks amplify aridity increase over land under global
1172 warming. *Nature Climate Change*. 6(9): 869-874, 2016. <https://doi.org/DOI: 10.1038/nclimate3029>.
- 1173 Beven, K., Germann, P. Macropores and water flow in soils revisited. *Water Resources Research*. 49(6):
1174 3071-3092, 2013. <https://doi.org/DOI: 10.1002/wrcr.20156>.
- 1175 Bouwer, H. Artificial recharge of groundwater: hydrogeology and engineering. *Hydrogeology Journal*.
1176 10(1): 121-142, 2002. <https://doi.org/DOI: 10.1007/s10040-001-0182-4>.
- 1177 Cai, H.E., Zhang, J.W., Zheng, J.G., Zhang, R.S., Liang, X.L. Hydrogeology features of Loess hilly gully
1178 region in Yan'an. *Geotechnical Engineering Technique*. 33(5): 288-292, 2019. [https://doi.org/DOI:](https://doi.org/DOI: 10.3969/j.issn.1007-2993.2019.05.009)
1179 [10.3969/j.issn.1007-2993.2019.05.009](https://doi.org/DOI: 10.3969/j.issn.1007-2993.2019.05.009).
- 1180 ~~Chen, P.Y., Ma, J.Z., Ma, X.Y., Yu, Q., Cui, X.K., Guo, J.B. Groundwater recharge in typical geomorphic
1181 landscapes and different land use types on the loess plateau, China. *Hydrological Processes*. 37(4): 14860-
1182 2023. <https://doi.org/DOI: 10.1002/hyp.14860>.~~
- 1183 Dane, J.H., Topp, C.G., Gee, G.W. 2.4 Particle-Size Analysis. 5: 255-293, 2002.
- 1184 Dasgupta, B., Prakash, P., Sen, R., Noble, J., Chatterjee, S., Sanyal, P. The isotopic composition of the
1185 world's highest river basins: Role of hydrological mixing ratios and transit time. *Journal of Hydrology*.
1186 638: 131544, 2024. <https://doi.org/DOI: 10.1016/j.jhydrol.2024.131544>.
- 1187 ~~Feng, X.M., Fu, B.J., Piao, S.L., Wang, S., Ciais, P., Zeng, Z.Z., Lü, Y.H., Zeng, Y., Li, Y., Jiang, X.H.,
1188 Wu, B.F. Revegetation in China's Loess Plateau is approaching sustainable water resource limits. *Nature
1189 Climate Change*. 6: 1019-1022, 2016. <https://doi.org/DOI: 10.1038/nclimate3092>.~~

1190 Fu, B.J., Chen, L., Ma, K. The effect of land use change on the regional environment in the Yangjuangou
1191 catchment in the loess plateau of China. *Acta Geographica Sinica*. 54: 241-246, 1999. [https://doi.org/DOI:](https://doi.org/DOI:10.3321/j.issn:0375-5444.1999.03.006)
1192 10.3321/j.issn:0375-5444.1999.03.006.

1193 Fu, B.J., Liu, Y., Lü, Y.H., He, C.S., Zeng, Y., Wu, B.F. Assessing the soil erosion control service of
1194 ecosystems change in the Loess Plateau of China. *Ecological Complexity*. 8 (4): 284-293, 2011.
1195 [https://doi.org/DOI: 10.1016/j.ecocom.2011.07.003](https://doi.org/DOI:10.1016/j.ecocom.2011.07.003).

1196 Fu, B.J., Wang, S., Liu, Y., Liu, J., Liang, W., Miao, C. Hydrogeomorphic ecosystem responses to natural
1197 and anthropogenic changes in the Loess Plateau of China. *Annual Review of Earth and Planetary*
1198 *Sciences*. 45: 223-243, 2017. [https://doi.org/DOI: 10.1146/annurev-earth-063016-020552](https://doi.org/DOI:10.1146/annurev-earth-063016-020552).

1199 Gates, J.B., Scanlon, B.R., Mu, X.M, Zhang, L. Impacts of soil conservation on groundwater recharge in
1200 the semi-arid Loess Plateau, China. *Hydrogeology Journal*. 19(4): 865-875, 2011. [https://doi.org/DOI:](https://doi.org/DOI:10.1007/s10040-011-0716-3)
1201 10.1007/s10040-011-0716-3.

1202 ~~Gee, G. W., Hillel, D. Groundwater recharge in arid regions: Review and critique of estimation methods.~~
1203 ~~*Hydrological Processes*. 2(3): 255-266, 1988. <https://doi.org/DOI:10.1002/hyp.3360020306>.~~

1204 Gleeson, T., Befus, K.M., Jasechko, S., Luijendijk, E., Cardenas, M.B. The global volume and
1205 distribution of modern groundwater. *Nature Geoscience*. 9(2): 161-167, 2016. DOI: 10.1038/NGEO2590.

1206 Gumuła-Kawęcka, A., Jaworska-Szulc B., Szymkiewicz A., Gorczewska-Langner W., Pruszkowska-
1207 Caceres M., Angulo-Jaramillo R., Šimůnek J. Estimation of groundwater recharge in a shallow sandy
1208 aquifer using unsaturated zone modeling and water table fluctuation method. *Journal of Hydrology*. 605:
1209 127283, 2022. DOI: 10.1016/j.jhydrol.2021.127283.

1210 He, M.N., Wang, Y.Q., Tong, Y.P., Zhao, Y.L., Qiang, X.K., Song, Y.G., Wang, L., Song, Y., Wang, G.D.,
1211 He, C.X. Evaluation of the environmental effects of intensive land consolidation: A field-based case
1212 study of the Chinese Loess Plateau. *Land Use Policy*. 94: 104523, 2020. DOI:
1213 10.1016/j.landusepol.2020.104523.

1214 Healy, R.W., Cook, P.G. Using groundwater levels to estimate recharge. *Hydrogeology Journal*. 10(1):
1215 91-109, 2002. DOI: 10.1007/s10040-001-0178-0.

1216 Heppner, C.S., Nimmo, J.R. A computer program for predicting recharge with a master recession curve.
1217 U.S. Geological Survey Scientific Investigations Report. 2005-5172, 2005. [https://doi.org/DOI:](https://doi.org/DOI:10.3133/sir20055172)
1218 10.3133/sir20055172.

1219 Huang, J., Li, Y., Fu, C., Chen, F., Fu, Q., Dai, A., Wang, G. Dryland climate change: Recent progress

1220 and challenges. *Reviews of Geophysics*. 55(3): 719-778, 2017. DOI: 10.1002/2016RG000550.

1221 [Huang L.M., Shao M.A. Advances and perspectives on soil water research in China's Loess Plateau.](#)

1222 [Earth-Science Reviews](#). 199(2): 102962, 2019. DOI: 10.1016/j.earscirev.2019.102962.

1223 [Huang, L.M., Wang, Z.W., Pei, Y.W., Zhu, X.C., Jia, X.X., Shao, M.A. Adaptive water use strategies of](#)

1224 [artificially revegetated plants in a water-limited desert: A case study from the Mu Us Sandy Land. Journal](#)

1225 [of Hydrology](#), 644: 132103, 2024. DOI: 10.1016/j.jhydrol.2024.132103.

1226 Huang, T.M., Pang, Z.H. Estimating groundwater recharge following land-use change using chloride

1227 mass balance of soil profiles: a case study at Guyuan and Xifeng in the Loess Plateau of China.

1228 *Hydrogeology Journal*. 19: 177-186, 2011. DOI: 10.1007/s10040-010-0643-8.

1229 Huang, T.M., Pang, Z.H., Edmunds, W.M. Soil profile evolution following land-use change: Implications

1230 for groundwater quantity and quality. *Hydrological Processes*. 27(8): 1238-1252, 2013. DOI:

1231 10.1002/hyp.9302.

1232 Huang, Y.N., Evaristo, J., Li, Z. Multiple tracers reveal different groundwater recharge mechanisms in

1233 deep loess deposits. *Geoderma*. 353: 207-212, 2019. DOI: 10.1016/j.geoderma.2019.06.041.

1234 Jasechko, S., Perrone, D. Global groundwater wells at risk of running dry. *Science*. 372(6540): 418-421,

1235 2021. DOI: 10.1126/science.abc2755.

1236 Ji, M.Y., Jia, D.B., Hao, Y.S., Liu, T., Yang, L.N., Li X.Y., Lv, C.G., Shang Z.Q. Hydrochemical and

1237 isotopic characteristics and water transformation relationships in the Zhenglan Banner section of

1238 Shandian River Basin. *Chinese Journal of Applied Ecology*. 1-11, 2024. DOI: 10.13287/j.1001-

1239 9332.202410.015.

1240 Jia, X.X., Zhu, P., Wei, X.R., Zhu, Y.J., Huang, M.B., Hu, W., Wang, Y.Q., Turkeltaub, T., Binley, A.,

1241 Horton, R., Shao, M.A. Bringing ancient loess critical zones into a new era of sustainable development

1242 goals. *Earth-Science Reviews*. 255: 104852, 2024. DOI: <https://doi.org/10.1016/j.earscirev.2024.104852>.

1243 Jin, Z., Guo, L., Wang, Y.Q., Yu, X.L., Lin, H., Chen, Y.P., Chu, G.C., Zhang, J., Zhang, N.P. Valley

1244 reshaping and damming induce water table rise and soil salinization on the Chinese Loess Plateau.

1245 *Geoderma*. 339: 115-125, 2019. DOI: <https://doi.org/10.1016/j.geoderma.2018.12.048>.

1246 Kuang, X.X., Luo, X., Jiao, J.J., Liang, S.H., Zhang, X.L., Li, H.L., Liu, J.G. Using stable isotopes of

1247 surface water and groundwater to quantify moisture sources across the Yellow River source region.

1248 *Hydrological Processes*. 33(13): 1835-1850, 2019. DOI: 10.1002/hyp.13441.

1249 Kumar, A., Sanyal, P., Agrawal, S. Spatial distribution of $\delta^{18}\text{O}$ values in river water in the Ganga River

1250 Basin: insight into the hydrological processes. *Journal of Hydrology*. 571: 225-234, 2019. DOI:
1251 10.1016/j.jhydrol.2019.01.044.

1252 Lai, J.S., Zou, Y., Zhang, J.L., Peres-Neto, P.R. Generalizing hierarchical and variation partitioning in
1253 multiple regression and canonical analyses using the rdacca.hp R package. *Methods in Ecology and*
1254 *Evolution*. 13(4): 782-788, 2022. DOI: 10.1111/2041-210X.13800.

1255 Lamontagne, S., Kirby, J., Johnston, C. Groundwater-surface water connectivity in a chain of ponds
1256 semiarid river. *Hydrological Processes*. 35(4): e14129, 2021. DOI: 10.1002/hyp.14129.

1257 Letz, O., Siebner, H., Avrahamov, N., Egozi, R., Eshel, G., Dahan, O. The impact of geomorphology on
1258 groundwater recharge in a semi-arid mountainous area. *Journal of Hydrology*. 603: 127029, 2021. DOI:
1259 10.1016/j.jhydrol.2021.127029.

1260 Li, H., Xiang, W., Si, B.C., Min, M., Miao, C.H., Jin, J.J. Quantifying recharge mechanisms in low-hilly
1261 areas of a loess region: Implications for the quantity and quality of groundwater. *Journal of Hydrology*.
1262 643: 131982, 2024a. DOI: 10.1016/j.jhydrol.2024.131982.

1263 [Li, M.Y., Xie, Y.Q., Dong, Y.H., Wang, L.H., Zhang, Z.Y. Review: Recent progress on groundwater](#)
1264 [recharge research in arid and semiarid areas of China. *Hydrogeology Journal*, 32\(1\), 9-30, 2024b. DOI:](#)
1265 [10.1007/s10040-023-02656-z.](#)

1266 Li, H.X., Han, S.B., Wu, X., Wang, S., Liu, W.P., Ma, T., Zhang, M.N., Wei, Y.T., Yuan, F.Q., Yuan, L.,
1267 Li, F.C., Wu, B., Wang, Y.S., Zhao, M.M., Yang, H.W., Wei, S.B. Distribution, characteristics and
1268 influencing factors of fresh groundwater resources in the Loess Plateau, China. *China Geology*. 4(3):
1269 209-526, 2021. DOI: 10.31035/cg2021057.

1270 Li, Y. S. Effects of forest on water circle on the Loess Plateau. *Journal of Natural Resources*. 16(05):
1271 427-432, 2001. DOI: 111451567011-81/4190641.

1272 Li, Y.R., Shi, W.H., Aydin, A., Beroya-Eitner, M.A., Gao, G.H. Loess genesis and worldwide distribution.
1273 *Earth-Science Reviews*. 201: 102947, 2020. DOI: <https://doi.org/10.1016/j.earscirev.2019.102947>.

1274 Li, Z., Chen, X., Liu, W.Z., Si, B.C. Determination of groundwater recharge mechanism in the deep
1275 loessial unsaturated zone by environmental tracers. *Science of The Total Environment*. 586: 827-835,
1276 2017. DOI: <https://doi.org/10.1016/j.scitotenv.2017.02.061>.

1277 Li, Z., Coles, A.E., Xiao, J. Groundwater and streamflow sources in China's Loess Plateau on catchment
1278 scale. *Catena*. 181: 104075, 2019. DOI: <https://doi.org/10.1016/j.catena.2019.104075>.

1279 Lian, H.S., Yen, H., Yu, K., Zou, J.Y., Liu, C.X. Groundwater pollution becomes new constraint after

1280 watershed-scale water quality restoration. *Journal of Hydrology*. 661: 133558, 2025. [DOI:](#)
1281 <https://doi.org/10.1016/j.jhydrol.2025.133558>.

1282 Liang, W., Bai, D., Wang, F.Y., Fu, B.J., Yan, J.P., Wang, S., Yang T.Y., Long, D., Feng, M.Q. Quantifying
1283 the impacts of climate change and ecological restoration on streamflow changes based on a Budyko
1284 hydrological model in China's Loess Plateau. *Water Resources Research*. 51: 6500-6519, 2015. DOI:
1285 10.1002/2014WR016589.

1286 Liang, X.J. *Applied hydrogeology*. Beijing: Science Press, 2016.

1287 Liu, D.S. *Loess and the environment*. Science Press, Beijing, 1985.

1288 Liu, X., Song, X.F., Zhang, Y.H., Xia, J., Zhang, X.C., Yu, J.J., Long, D., Li, F.D., Zhang, B. Spatio-
1289 temporal variations of $\delta^2\text{H}$ and $\delta^{18}\text{O}$ in precipitation and shallow groundwater in the Hilly Loess Region
1290 of the Loess Plateau, China. *Environmental Earth Sciences*. 63(5): 1105–1118, 2011. DOI:
1291 10.1007/s12665-010-0785-y.

1292 Liu, Y.S., Chen, Z., Li, Y., Feng, W., Cao, Z. The planting technology and industrial development
1293 prospects of forage rape in the loess hilly area: A case study of newly-increased cultivated land through
1294 gully land consolidation in Yan'an, Shaanxi Province. *Journal of Natural Resources*. 32: 2065-2074, 2017.
1295 DOI: 10.11849/zrzyxb.20161142.

1296 Liu, Y.S., Li, Y. Engineering philosophy and design scheme of gully land consolidation in Loess Plateau.
1297 *Transactions of the Chinese Society of Agricultural Engineering*. 33(10): 1-9, 2017. [DOI:](#)
1298 [10.11975/j.issn.1002-6819.2017.10.001](https://doi.org/10.11975/j.issn.1002-6819.2017.10.001)

1299 [Liu, Y.Z. Source analysis of precipitation chemical components on the Loess Plateau based on hydrogen](#)
1300 [and oxygen stable isotopes\[D\]. Northwest A&F University, 2024.](#)
1301 [DOI:10.27409/d.cnki.gxbnu.2024.001528](https://doi.org/10.27409/d.cnki.gxbnu.2024.001528).

1302 Lu, Y.W. Study on typical hydrological characteristics of the vadose zone and spatiotemporal evolution
1303 of potential groundwater recharge in the Chinese Loess Plateau. Yangling: Northwest A & F University,
1304 2020. DOI: 10.11975/j.issn.1002-6819.2017.10.001.

1305 Lupi, L., Bertrand, L., Monferrán, M. V., Amé, M. V., del Pilar Diaz, M. Multilevel and structural
1306 equation modeling approach to identify spatiotemporal patterns and source characterization of metals
1307 and metalloids in surface water and sediment of the Ctalamochita River in Pampa region, Argentina.
1308 *Journal of Hydrology*. 572: 403-413, 2019. [https://doi.org/DOI: 10.1016/j.jhydrol.2019.03.019](https://doi.org/10.1016/j.jhydrol.2019.03.019).

1309 Manna, F., Murray, S., Abbey, D., Martin, P., Cherry, J., Parker, B. Spatial and temporal variability of

1310 groundwater recharge in a sandstone aquifer in a semi-arid region. *Hydrology and Earth System Sciences*
1311 *Discussions*. 2018: 1-36, 2018. <https://doi.org/DOI:10.5194/hess-23-2187-2019>.

1312 Medici, G., Munn, J. D., Parker, B. L. Delineating aquitard characteristics within a Silurian dolostone
1313 aquifer using high-density hydraulic head and fracture datasets. *Hydrogeology Journal*. 32(6): 1663-1691,
1314 2024. DOI: <https://doi.org/10.1007/s10040-024-02824-9>.

1315 Meles, M.B., Bradford, S., Casillas-Trasvina, A., Chen, L., Osterman, G., Hatch, T., Ajami, H., Crompton,
1316 O., Levers, L., Kisekka, I. Uncovering the gaps in managed aquifer recharge for sustainable groundwater
1317 management: A focus on hillslopes and mountains. *Journal of Hydrology*. 639: 131615, 2024. DOI:
1318 10.1016/j.jhydrol.2024.131615.

1319 Nachabe, M.H. Analytical expressions for transient specific yield and shallow water table drainage.
1320 *Water Resources Research*. 38 (10): 11-17, 2002. DOI: 10.1029/2001WR001071.

1321 Nicholson, S. E. *Dryland Climatology*. Cambridge University Press, 2011.

1322 Obuobie, E., Diekkruieger, B., Agyekum, W., Agodzo, S. Groundwater level monitoring and recharge
1323 estimation in the White Volta River basin of Ghana. *Journal of African Earth Sciences*. 71-72: 80-86,
1324 2012. DOI: 10.1016/j.jafrearsci.2012.06.005.

1325 Ouali, A.E., Roubil, A., Lahrach, A., Hmadi, A.E., Ouali, A.E., Ousmana, H., Bouchaou, L. Assessments
1326 of groundwater recharge process and residence time using hydrochemical and isotopic tracers under arid
1327 climate: Insights from Errachidia basin (Central-East Morocco). *Groundwater for Sustainable*
1328 *Development*. 25: 101145, 2024. DOI: 10.1016/j.gsd.2024.101145.

1329 Owuor, S. O., Butterbach-Bahl, K., Guzha, A. C., Rufino, M. C., Pelster, D. E., Díaz-Pinés, E., Breuer,
1330 L. Groundwater recharge rates and surface runoff response to land use and land cover changes in semi-
1331 arid environments. *Ecological Processes*, 5: 1-21, 2016. DOI: 10.1186/s13717-016-0060-6.

1332 Pe'csi, M. Loess is not just the accumulation of dust. *Quat Int.* 7(8):1-21, 1990. DOI:10.1016/1040-
1333 6182(90)90034-2.

1334 Qiao, J.B., Zhu, Y.J., Jia, X.X., Huang, L.M., Shao, M.A. Spatial variability of soil water for the entire
1335 profile in the critical zone of the Loess Plateau. *Advances in Water Science*. 28(04): 515-522, 2017. DOI:
1336 10.14042/j.cnki.32.1309.2017.04.005.

1337 Qu, S., Zhao, Y.Z., Li, M.H., Ren, X.H., Wang, C.Y., Yang, X., Hao, Y.L., Dong, S.G., Yu, R.H. Unveiling
1338 sources and fate of sulfate in lake-groundwater system combined Bayesian isotope mixing model with
1339 radon mass balance model. *Water Research*. 282: 123648, 2025. DOI: 10.1016/j.watres.2025.123648.

1340 Salek, M., Levison, J., Parker, B., Gharabaghi, B. CAD-DRASTIC: chloride application density
1341 combined with DRASTIC for assessing groundwater vulnerability to road salt application. *Hydrogeology*
1342 *Journal*. 26: 2379-2393, 2018. DOI: 10.1007/s10040-018-1801-7.

1343 Scanlon, B.R., Healy, R.W., Cook, P.G. Choosing appropriate techniques for quantifying groundwater
1344 recharge. *Hydrogeology Journal*. 10(1): 18-39, 2002. DOI: 10.1007/s10040-001-0176-2.

1345 Shah, N., Ross, M. Variability in specific yield under shallow water table conditions. *Journal of*
1346 *Hydrologic Engineering*. 14(12): 1290-1298, 2009. DOI: [https://doi.org/10.1061/\(ASCE\)HE.1943-](https://doi.org/10.1061/(ASCE)HE.1943-5584.0000121)
1347 [5584.0000121](https://doi.org/10.1061/(ASCE)HE.1943-5584.0000121).

1348 Shi, H., Shao, M.A. Soil and water loss from the Loess Plateau in China. *Journal of arid environments*.
1349 45(1): 9-20, 2002. DOI: <https://doi.org/10.1006/jare.1999.0618>.

1350 ~~Shi, P.J., Huang, Y.N., Yang, K.Y., Li, Z. Quantitative estimation of groundwater recharge in the thick~~
1351 ~~loess deposits using multiple environmental tracers and methods. *Journal of Hydrology*. 603(8): 126895,~~
1352 ~~2021. DOI: <https://doi.org/10.1016/j.jhydrol.2021.126895>.~~

1353 Tan, H.B., Liu, Z.H., Rao, W.B., Jin, B., Zhang, Y.D. Understanding recharge in soil-groundwater
1354 systems in high loess hills on the Loess Plateau using isotopic data. *Catena*. 156: 18-29, 2017. DOI:
1355 <https://doi.org/10.1016/j.catena.2017.03.022>.

1356 Tan, H.B., Wen, X.W., Rao, W.B., Bradd, J., Huang, J.Z. Temporal variation of stable isotopes in a
1357 precipitation-groundwater system: implications for determining the mechanism of groundwater recharge
1358 in high mountain hills of the Loess Plateau, China. *Hydrological Processes*. 30(10): 1491-1505, 2016.
1359 DOI: <https://doi.org/10.1002/hyp.10729>.

1360 Tetzlaff, D., Seibert, J., McGuire, K.J., Laudon, H., Burns, D.A., Dunn, S.M., Soulsby, C. How does
1361 landscape structure influence catchment transit time across different geomorphic provinces?
1362 *Hydrological Processes*. 23: 945-953, 2009. DOI: <https://doi.org/10.1002/hyp.7240>.

1363 Tooth, S. Arid geomorphology: Changing perspectives on timescales of change. *Progress in Physical*
1364 *Geography*. 36(2): 262-284, 2012. DOI: 10.1177/0309133311417943.

1365 Vries, J.J.D., Simmers, I. Groundwater recharge: an overview of processes and challenges. *Hydrogeology*
1366 *Journal*. 10(1): 5-17, 2002. DOI: 10.1007/s10040-001-0171-7.

1367 Wan, H., Liu, W.G. An isotope study ($\delta^{18}\text{O}$ and $\delta^2\text{H}$) of water movements on the Loess Plateau of China
1368 in arid and semiarid climates. *Ecological Engineering*. 8(93): 226-233, 2016. DOI:
1369 <https://doi.org/10.1016/j.ecoleng.2016.05.039>

1370 Wang, L., Shao, M., Wang, Q.J., Gale, J. Historical changes in the environment of the Chinese Loess
1371 Plateau. *Environmental Science & Policy*. 9: 675-684, 2006. DOI:
1372 <https://doi.org/10.1016/j.envsci.2006.08.003>.

1373 Wang, W.Z., Sun, J.N., Xia, Y., Li, Z. Identifying hydraulic connectivity among the vadose zone,
1374 unconfined and confined aquifers in the thick loess deposits using multiple tracers. *Journal of Hydrology*.
1375 626: 130339, 2023. DOI: <https://doi.org/10.1016/j.jhydrol.2023.130339>.

1376 Wang, W.Z., Xia, Y., Sun, J.N., Liu, Y.Z., Li, P.Y., Han, F.P., Li, Z. Uncertainties in physical and tracer
1377 methods in actual groundwater recharge estimation in the thick loess deposits of China. *Journal of*
1378 *Hydrology*. 634: 131127, 2024. DOI: <https://doi.org/10.1016/j.jhydrol.2024.131127>.

1379 Wang, Y.Q., Shao, M.A., Sun, H., Fu, Z.H., Fan, J., Hu, W., Fang, L.C. Response of deep soil drought to
1380 precipitation, land use and topography across a semiarid watershed. *Agricultural and Forest Meteorology*.
1381 282-283: 107866, 2020. DOI: <https://doi.org/10.1016/j.agrformet.2019.107866>.

1382 ~~Wang, Y.Q., Sun, H., Zhao, Y.L. Characterizing spatial-temporal patterns and abrupt changes in deep soil~~
1383 ~~moisture across an intensively managed watershed. *Geoderma*. 341: 181-194, 2019. DOI:~~
1384 ~~<https://doi.org/10.1016/j.geoderma.2019.01.044>.~~

1385 Wu, M.L. The structural equation model: AMOS operation and application. Chongqing: Chongqing
1386 University Press, 2010.

1387 Xiang W. Study on soil evaporation and groundwater recharge based on stable isotopes in the Loess
1388 Plateau at regional scale. Yangling: Northwest A & F University, 2020. DOI:
1389 10.27409/d.cnki.gxbnu.2021.000025.

1390 [Xiang, W., Si, B.C., Biswas, A., Li, Z. Quantifying dual recharge mechanisms in deep unsaturated zone](https://doi.org/10.1016/j.geoderma.2018.10.006)
1391 [of Chinese Loess Plateau using stable isotopes. *Geoderma*. 337: 773-781, 2019. DOI:](https://doi.org/10.1016/j.geoderma.2018.10.006)
1392 [10.1016/j.geoderma.2018.10.006](https://doi.org/10.1016/j.geoderma.2018.10.006).

1393

1394 Xie, T.T., Zhao, H.J., Chen, G.K., Lin, H.H. Land Use Patterns and River Nitrate Dynamics in Karst
1395 Regions: Insights from High-Resolution Sentinel-2 Imagery and Partial Least Squares Structural
1396 Equation Modeling Analysis. *Environmental Engineering Science*, 2025. DOI:
1397 <https://doi.org/10.1089/ees.2024.0272>.

1398 Xu, P., Weng, B.S., Gong, X.Y., Xia, K.B., Yan, D.H., Wang, H. Estimation of shallow groundwater
1399 recharge in central Qinghai-Tibet Plateau by combining unsaturated zone simulation and improved water

1400 table fluctuation method. Journal of Hydrology. 630: 130689, 2024. DOI:
1401 <https://doi.org/10.1016/j.jhydrol.2024.130689>.

1402 Xu, Y., Beekman, H. E. Review: Groundwater recharge estimation in arid and semi-arid southern Africa.
1403 Hydrogeology Journal. 27(3): 929-943, 2019. DOI: 10.1007/s10040-018-1898-8.

1404 Xu, Z.Y., Zhao, Y.J., Chen, J.J. Research of fractural efficacy on mechanisms governing water flow in
1405 unsaturated loess. Journal of Changchun University of Earth Scienses. 23(03): 326-329, 1993.

1406 Xue, S.B., Li, P., Cui, Z.W., Li, Z.B. The influence of different check dam configurations on the
1407 downstream river topography and water-sediment relationship. Journal of Hydrology. 656: 133046, 2025.
1408 DOI: 10.1016/j.jhydrol.2025.133046.

1409 ~~Yan, T.B., Wang, D.Q. The Recharge Mechanism of Unconfined Groundwater in the Loess of the~~
1410 ~~Luochuan Yuan and Its Water Bearing Characteristics. Geological Review. 5(29): 418-427, 1983. DOI:~~
1411 ~~[10.16509/j.georeview.1983.05.003](https://doi.org/10.16509/j.georeview.1983.05.003)~~

1412 Yang, N., Wang, G.C. Spatial variation of water stable isotopes of multiple rivers in southeastern Qaidam
1413 Basin, northeast Qinghai-Tibetan Plateau: Insights into hydrologic cycle. Journal of Hydrology. 628:
1414 130464, 2023. [https://doi.org/DOI: 10.1016/j.jhydrol.2023.130464](https://doi.org/10.1016/j.jhydrol.2023.130464).

1415 ~~Yang, X.P., Liu, T., Yuan, B.Y. The Loess Plateau of China: Aeolian sedimentation and fluvial erosion,~~
1416 ~~both with superlative rates. Geomorphological Landscapes of the World. 1: 275-282, 2009. DOI:~~
1417 ~~[10.1007/978-90-481-3055-9_28](https://doi.org/10.1007/978-90-481-3055-9_28).~~

1418 Yu L.L., Ji, Z.X., Wang, L. Characteristics of Perched Water Recharge in the Dam Land of Yangjuangou
1419 Small Watershed on the Loess Plateau. Acta Pedologica Sinica. 62(4): 983-997, 2025. DOI :
1420 10.11766/trxb202404290178.

1421 [Yu, Y.L., Jin, Z., Chu, G.C., Zhang, J., Wang, Y.Q., Zhao, Y.L. Effects of valley reshaping and](https://doi.org/10.1016/j.jhydrol.2020.124702)
1422 [damming on surface and groundwater nitrate on the Chinese Loess Plateau. Journal of Hydrology.](https://doi.org/10.1016/j.jhydrol.2020.124702)
1423 [584: 124702, 2020.](https://doi.org/10.1016/j.jhydrol.2020.124702)

1424 ~~Yuan, S., Li, Z., Chen, L., Li, P., Zhang, Z., Zhang, J., Wang, A. Effects of a check dam system on the~~
1425 ~~runoff generation and concentration processes of a catchment on the Loess Plateau. International Soil~~
1426 ~~and Water Conservation Research. 10(1): 86-98, 2022. [https://doi.org/DOI: 10.1016/j.iswer.2021.06.007](https://doi.org/10.1016/j.iswer.2021.06.007).~~

1427 Zhang, H., Xu, Y.X., Kanyerere, T. A review of the managed aquifer recharge: Historical development,
1428 current situation and perspectives. Physics and Chemistry of the Earth, Parts A/B/C. 118-119: 102887,
1429 2020. DOI: 10.1016/j.pce.2020.102887.

1430 Zhang, J., Chen, H.S., Fu, Z.Y., Wang, F., Wang, K.L. Towards hydrological connectivity in the karst
1431 hillslope critical zone: Insight from using water isotope signals. *Journal of Hydrology*. 617: 128926, 2022.
1432 DOI: 10.1016/j.jhydrol.2022.128926.

1433 Zhang, Y.H., Wu, Y.P. Oxygen and Hydrogen Isotopes in Precipitation in Heihe River Basin, China.
1434 *Journal of Glaciology and Geocryology*. 31(1): 34-39, 2009. DOI: 100020240(2009)0120034206.

1435 [Zhao, Y., Wang, L. Determination of groundwater recharge processes and evaluation of the “two water](#)
1436 [worlds” hypothesis at a check dam on the Loess Plateau. *Journal of Hydrology*. 595: 125989, 2021. DOI:](#)
1437 [10.1016/j.jhydrol.2021.125989.](#)

1438 Zhao, Y. L., Wang, Y.Q., Sun, H., Lin, H., Jin, Z., He, M.N., Yu, Y. L., Zhou, W. J., and An, Z. S. Intensive
1439 land restoration profoundly alters the spatial and seasonal patterns of deep soil water storage at watershed
1440 scales. *Agriculture, Ecosystems & Environment*. 280: 129-141, 2019. [https://doi.org/DOI:](https://doi.org/10.1016/j.agee.2019.04.028)
1441 [10.1016/j.agee.2019.04.028.](https://doi.org/10.1016/j.agee.2019.04.028)

1442 ~~[Zhao, Y., Wang, L. Determination of groundwater recharge processes and evaluation of the ‘two water](#)
1443 ~~[worlds’ hypothesis at a check dam on the Loess Plateau. *Journal of Hydrology*. 595: 125989, 2021.](#)~~
1444 ~~[https://doi.org/10.1016/j.jhydrol.2021.125989.](https://doi.org/10.1016/j.jhydrol.2021.125989)~~~~

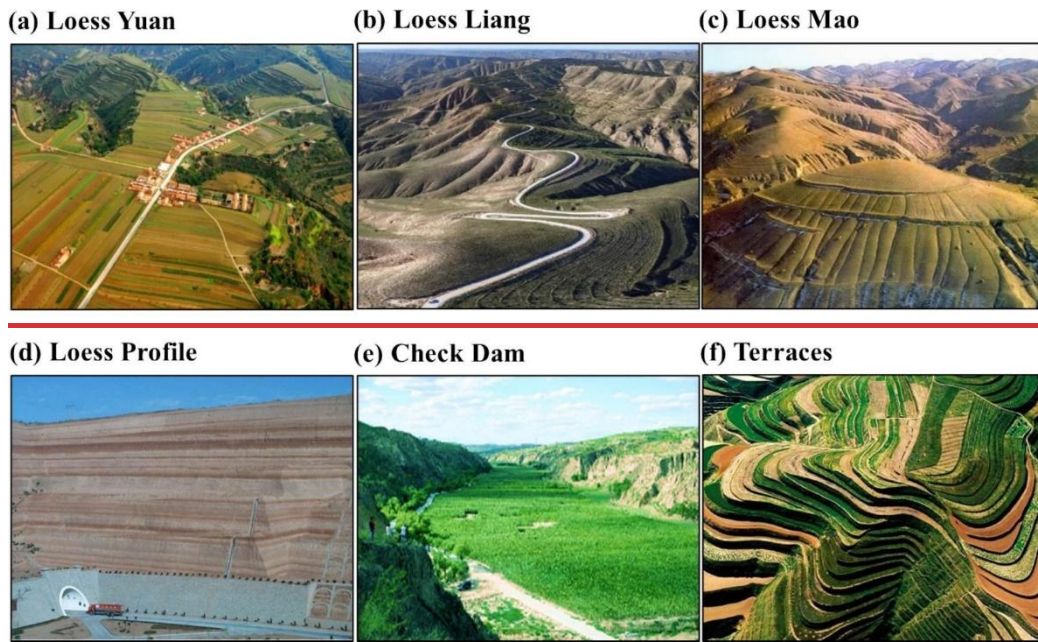
1445 ~~[Zhao, Y.L., Wang, Y.Q., Hu, W., Sun, H., Qi, L.J., Xu, L., Song, Y., Zhang, P.P. Intensive land restoration](#)
1446 ~~[projects alter mechanisms underpinning spatiotemporal soil moisture variability at a catchment scale: A](#)~~
1447 ~~[case study in China. *Journal of Hydrology*. 630: 130739, 2024. \[https://doi.org/DOI:\]\(https://doi.org/10.1016/j.jhydrol.2024.130739\)](#)~~
1448 ~~[10.1016/j.jhydrol.2024.130739.](https://doi.org/10.1016/j.jhydrol.2024.130739)~~~~

1449 Zhao, Y.L., Wang, Y.Q., Zhou, J.X., Qi, L.J., Zhang, P.P. Spatiotemporal variation and controlling factors
1450 of dried soil layers in a semi-humid catchment and relevant land use management implications. *CATENA*.
1451 240: 107973, 2024. [https://doi.org/DOI: 10.1016/j.catena.2024.107973.](https://doi.org/10.1016/j.catena.2024.107973)

1452 Zhu, Y.J., Jia, X.X., Shao, M.A. Loess thickness variations across the loess plateau of China. *Surveys in*
1453 *Geophysics*. 39(4): 715-727, 2018. [https://doi.org/DOI: 10.1007/s10712-018-9462-6.](https://doi.org/10.1007/s10712-018-9462-6)

1454 **Appendix A**

1455 ~~1. The typical loess landforms on the Loess Plateau is shown-~~



1456

1457 ~~Fig. A1. Typical loess landforms are (a) Loess Yuan, (b) Loess Liang, and (c) Loess Mao. (d) A loess~~
 1458 ~~profile, (e) check dams and (f) terraces on the Chinese Loess Plateau. (adapted from Jia et al., 2024)~~

1459 ~~21. The specific yield of different soil textures is shown.~~

1460 Table A1. The specific yield of different texture of soil (adapted from Liang, 2016)

Texture	Average Specific Yield	Minimum Specific Yield	Maximum Specific Yield	Coefficient of Variation (%)
Clay	0.02	0.00	0.05	59
Silt	0.08	0.03	0.19	60
Sandy Clay	0.07	0.03	0.12	44
Fine Sand	0.21	0.10	0.28	32
Medium Sand	0.26	0.15	0.32	18
Coarse Sand	0.27	0.20	0.35	18
Gravelly Sand	0.25	0.20	0.35	21
Fine Gravel	0.25	0.21	0.35	18
Medium Gravel	0.23	0.13	0.26	14
Coarse Gravel	0.22	0.12	0.26	20

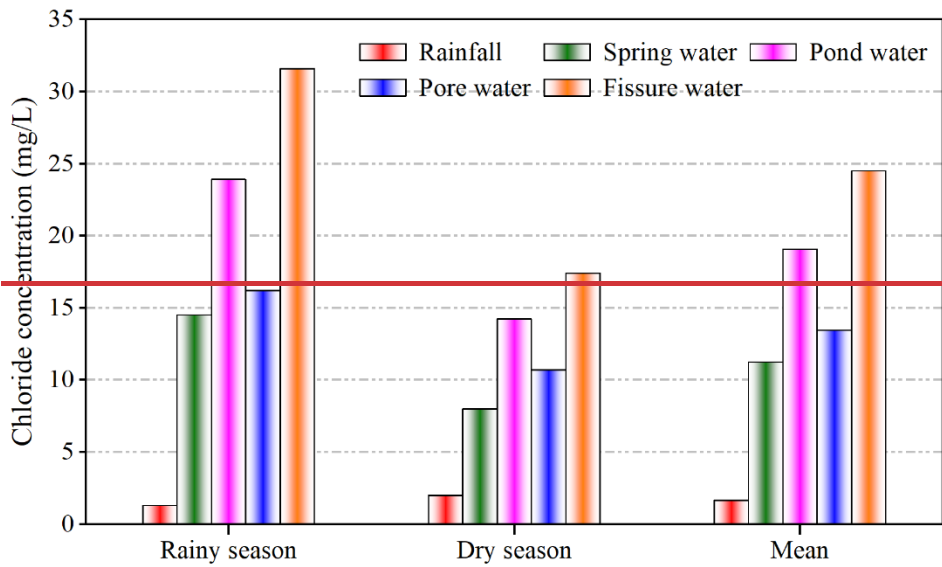
1461

1462 32. The isotopic composition ($\delta^2\text{H}$ and $\delta^{18}\text{O}$) of various water sources in the rainy and dry seasons is
1463 shown.

1464 Table A2. Isotopic composition ($\delta^2\text{H}$ and $\delta^{18}\text{O}$) of various water sources in the rainy and dry seasons

	Rainy season		Dry season	
	$\delta^2\text{H}$	$\delta^{18}\text{O}$	$\delta^2\text{H}$	$\delta^{18}\text{O}$
Rainfall	$-36.6\pm 20.4\text{‰}$	$-5.6\pm 2.3\text{‰}$	$-31.0\pm 23.2\text{‰}$	$-4.9\pm 3.0\text{‰}$
Pond water	$-40.5\pm 13.1\text{‰}$	$-4.1\pm 2.3\text{‰}$	$-24.5\pm 6.9\text{‰}$	$-0.8\pm 1.3\text{‰}$
Spring water	$-67.3\pm 2.6\text{‰}$	$-9.0\pm 0.4\text{‰}$	$-68.4\pm 2.2\text{‰}$	$-9.0\pm 0.4\text{‰}$
Pore water	$-66.3\pm 3.1\text{‰}$	$-9.0\pm 0.6\text{‰}$	$-65.4\pm 3.8\text{‰}$	$-8.5\pm 0.6\text{‰}$
Fissure water	$-65.0\pm 3.8\text{‰}$	$-8.8\pm 0.9\text{‰}$	$-64.5\pm 5.5\text{‰}$	$-8.5\pm 0.9\text{‰}$

1465 4. The chloride concentrations of various water sources in the rainy and dry seasons is shown.



1466

1467 Fig. A2. Chloride concentrations of various water sources in the rainy and dry seasons.